Mineralogy and Petrology (2021) 115:445–466
https://doi.org/10.1007/s00710-021-00745-z

ORIGINAL PAPER

Mafic to intermediate composition intrusions from the Kahak area, central Urumieh-Dokhtar arc of Iran: transition from Eocene to Miocene intra-arc extensional magmatism

Sakine Moradi[1] · Mohammad Reza Ghorbani[1] · Shao-Yong Jiang[2] · Eric H. Christiansen[3]

Received: 18 January 2020 / Accepted: 2 March 2021 / Published online: 18 March 2021

Abstract

Several gabbro, gabbroic diorite, and diorite intrusions were emplaced in the Neotethyan Urumieh-Dokhtar magmatic arc in the Kahak area of the Zagros Orogen. The plutonic rocks intruded Cenozoic volcanic and pyroclastic succession. U-Pb dating via LA-ICP-MS of zircon yields early to middle Eocene ages of ~53 to 38 Ma for the diorite and gabbroic diorite in Veshnaveh and Naragh areas and Miocene ages of 23 to 20 Ma for gabbroic rocks in the Kerogan and Fordou areas. The Eocene magmatic phase occurred quite possibly as three continuous pulses. The Eocene and Miocene intrusions have negative Nb-Ta anomalies like those of subduction-related magmas. The Pb isotopic compositions show the involvement of subducted sediment in the source of the studied samples. The Eocene intrusions are tholeiitic and enriched in incompatible-trace-elements (especially the HFSE) compared to the Miocene intrusions which are calc-alkaline and have lower concentrations of most incompatible trace elements. Sr-Nd isotopic compositions of the Eocene rocks lie close to the mantle array and near Bulk Silicate Earth, but the Miocene suite is shifted to higher $(^{87}Sr/^{86}Sr)_i$. The higher $(^{87}Sr/^{86}Sr)_i$, along with larger Ba, K, Pb, and Sr anomalies, in the Miocene suite imply more slab fluid input and/or crustal contamination. Apparently, the Eocene mafic magmas formed in slightly metasomatized subcontinental lithospheric mantle (SCLM), whereas the Miocene suite was derived from highly metasomatized, deeper levels of the SCLM. We suggest that slab roll back occurred between the Eocene and Miocene and transferred the location of mantle partial melting to greater depths.

Keywords U-Pb dating · Subcontinental lithospheric mantle · Slab roll-back · Trace element geochemistry · Urumieh-Dokhtar magmatic arc · Iran

Introduction

The geochemistry of mafic to intermediate igneous rocks provides an important means to understand tectonic events (especially in subduction zones), magma sources, and melting conditions (Kamei et al. 2004; Karsli et al. 2010) as well as the growth and differentiation of continental crust. Potential mantle sources of mafic-intermediate rocks on the continents are varied and include subcontinental lithospheric mantle, plume-related ocean island basalt (OIB) type mantle, or depleted mid-ocean ridge basalt (normal or N-MORB) type asthenospheric mantle. In convergent zones, fluids and melts released from subducting slabs and the subducted sediments may also be involved in magma generation (Saunders 2005; Garfunkel 2008).

Mafic to intermediate composition intrusions constitute a significant portion of the Cenozoic Urumieh-Dokhtar Magmatic Arc (UDMA) of Iran (see Appendix in Ghorbani 2006) which is largely composed of a volcanic succession that is up to 2000 m thick. Based on the interlayered fossiliferous beds in the UDMA, the magmatic assemblage was thought to be Eocene in age (e.g., Hajian

Editorial handling: Q. Wang

✉ Mohammad Reza Ghorbani
ghorbani@modares.ac.ir

[1] Department of Geology, Tarbiat Modares University, Tehran, Jalal Al Ahmad 14115-175, Iran

[2] State Key Laboratory of Geological Processes and Mineral Resources, Faculty of Earth Resources, Collaborative Innovation Center for Exploration of Strategic Mineral Resources, China University of Geosciences, Wuhan 430074, China

[3] Department of Geological Sciences, Brigham Young University, Provo, UT 84602-4606, USA

2001). However, in recent years multiple reports about Oligocene and Miocene magmatic rocks from the UDMA have been provided (e.g., Chiu et al. 2013; Yeganehfar et al. 2013; Ghorbani et al. 2014). The mafic magmas of the UDMA are believed to have been derived from the mantle in a magmatic arc (e.g., Babazadeh et al. 2017; Honarmand et al. 2014). Locally, these mafic magmas experienced differentiation, combined with different degree of crustal assimilation, to produce granitic intrusions.

The UDMA was originally thought to be composed of calc-alkaline rocks (e.g., Berberian et al. 1982). However, recent works show that the mafic-intermediate intrusions are mainly tholeiitic, at least in some areas (Yeganehfar et al. 2013; Ghorbani et al. 2014; Babazadeh et al. 2017). Some alkaline rocks (Hassanzadeh 1993 and Moradian Shahr-e-babaky 1997) including minor ultrapotassic and shoshonitic rocks (Aftabi and Atapour 2000) are also present.

Because of the tholeiitic, calc-alkaline, and alkaline geochemical affinities, as well as significant trace element variability of the UDMA rocks, a range of subduction-related settings have been invoked to account for petrogenesis of the magmatic rocks. For example, the Eocene magmatic rocks in the UDMA have been attributed to a magmatic flare-up involving widespread decompression melting of lithospheric mantle which had been metasomatized by slab-derived fluids (Verdel et al. 2011). Oligocene and Miocene magmatism has been attributed to upwelling and melting of asthenospheric mantle that experienced some modification by fluids released from a subducting slab of lithosphere (Verdel et al. 2011; Ghorbani et al. 2014) during slab roll-back (Ghorbani and Bezenjani 2011; Yeganehfar et al. 2013). Considering the scarcity of radiometric ages and isotopic data, details of the sources and processes involved in the generation and evolution of the UDMA magmas are poorly constrained.

The major scientific goal of this study is a reappraisal of the geochemical evolution of intrusive rocks through time in the Kahak area of the UDMA. Trace element differences between the Eocene and Miocene intrusive rocks are of particular note and provide clues to the tectonic evolution of the larger region. Our study employs major and trace element, and Sr-Nd-Pb isotopic characteristics of the mafic-intermediate intrusive rocks from the Kahak area (Fig. 1), and for the first time provides U-Pb zircon ages. The geochemical and geochronological data are used to elucidate the sources and processes involved in the development of this magmatic belt in the Eocene and Miocene.

Regional geology

The Zagros Orogen is part of the Alpine-Himalayan belt and extends from northwest to southeast Iran. The Zagros belt formed by closure of the Neotethyan Ocean and eventual collision of the Arabian and Eurasian plates along the western margin of the Central Iran plate. The orogenic belt is subdivided into three parts (Fig. 1a); from NE to SW these are: the Urumieh-Dokhtar Magmatic Arc (UDMA), the Sanandaj-Sirjan Zone (SSZ), and the Zagros Fold and Thrust Belt (ZFTB).

The UDMA is considered to have formed from a voluminous, and distinctly linear, Andean-style magmatic arc system (Dewey et al. 1973) that formed on the active SW margin of the Iranian plate during the Cenozoic (Arvin et al. 2007). Omrani et al. (2008) subdivided the UDMA volcanic rocks into an older Eocene suite and a younger upper Miocene to Plio-Quaternary suite. The Middle Eocene was thought to include the peak of magmatic activity in the region (Berberian and King 1981; Ghasemi and Talbot 2006). The Miocene igneous rocks of the UDMA were considered to mark the continental collision between Arabia and Eurasia (Berberian and King 1981; Allen et al. 2004; Ballato et al. 2011; Mohajjel and Fergusson 2014). On the other hand, Mouthereau et al. (2012) suggested that collision began in the late Eocene at ~35 Ma, was followed by crustal thickening in the Oligocene, and uplift of the central Iranian plateau in the Middle Miocene (15–12 Ma) prior to slab breakoff.

Recently, many Oligocene volcanic and plutonic bodies have also been found in the UDMA that provide more details about the geodynamic evolution of this assemblage (Fig. 2 in Babazadeh et al. 2018 and references therein). The geochemical characteristics of the Oligocene and Miocene igneous rocks in the UDMA indicate a continuous supply of magma from subduction-related sources. Rare adakitic and Nb-Ta enriched rocks of Oligocene-Miocene age in the UDMA do not have typical collision signatures either (Yeganehfar et al. 2013; Ghorbani et al. 2014). In light of these data, more recent studies have emphasized the role of Neotethyan roll-back of the subducting slab and subsequent asthenospheric upwelling to generate late Oligocene and Miocene magmatism (Babazadeh et al. 2017; Ghorbani et al. 2014; Verdel et al. 2011; Yeganehfar et al. 2013). In this model, collision occurred later than the Miocene.

The study area 25 km south Kahak in the central UDMA (Fig. 1), comprises vast outcrops of Eocene to Miocene volcano-sedimentary successions (Ghalamghash and Babakhani 1996). Eocene volcanic units are dominant. The major rock types are gray to reddish tuffs along with rhyolitic, dacitic, and andesitic lavas and dykes that are interbedded with nummulitic limestone. Multiple bodies of magmatic rock intruded the Eocene volcano-sedimentary successions. Most of these intrusions (Bidhand, Veshnaveh, Fordou, Naragh and Kerogan) are stocks to small batholiths in size, whereas the Naragh intrusions are sills. The intrusions range from gabbroic (from Bidhand and Kerogan) to dioritic (from Veshnaveh) in composition. The Fordou intrusions tend toward monzogabbro.

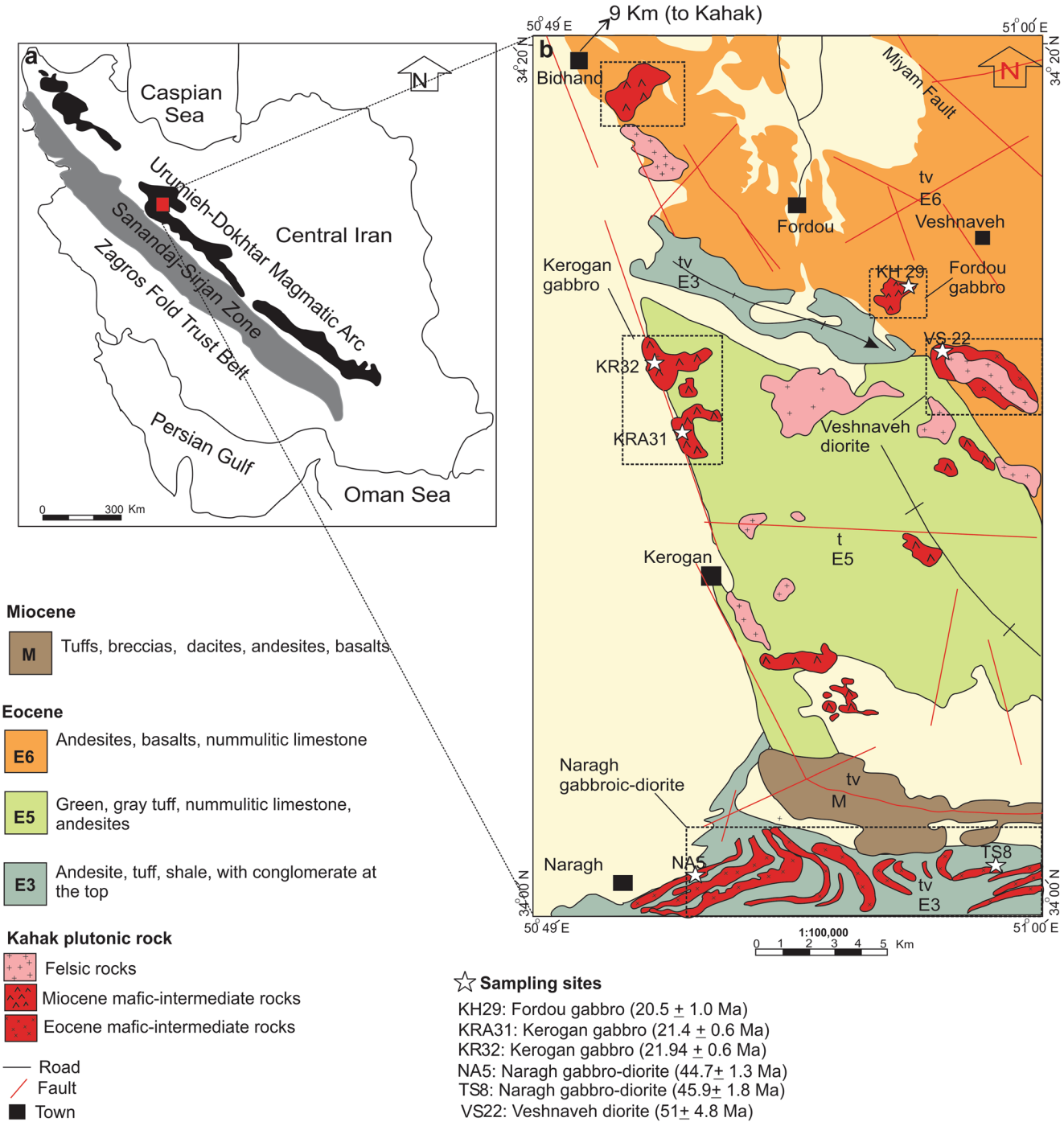

Fig. 1 **a** A map of Iran showing major tectonomagmatic units of the Zagros belt (modified after Alavi 1996); **b** mafic to intermediate composition intrusive bodies (Eocene Naragh and Veshnaveh intrusions and Miocene Kerogan, Bidhand, and Fordou intrusions) from the Kahak area of central UDMA are shown on a geological map (modified after Ghalamghash and Babakhani 1996). Locations of the U-Pb age dated samples are also shown

Analytical methods

Zircon U-Pb geochronology

Zircon grains were separated from 6 samples (Naragh samples TS8, NA5, Veshnaveh sample VSA21, Kerogan samples KRA32, KR31, and Fordou sample KH29). The zircon grains from the Kahak mafic-intermediate intrusive rocks were hand-picked under a binocular microscope after crushing and conventional magnetic and heavy liquid separation. Then they were mounted in epoxy resin and polished to approximately half their thickness.

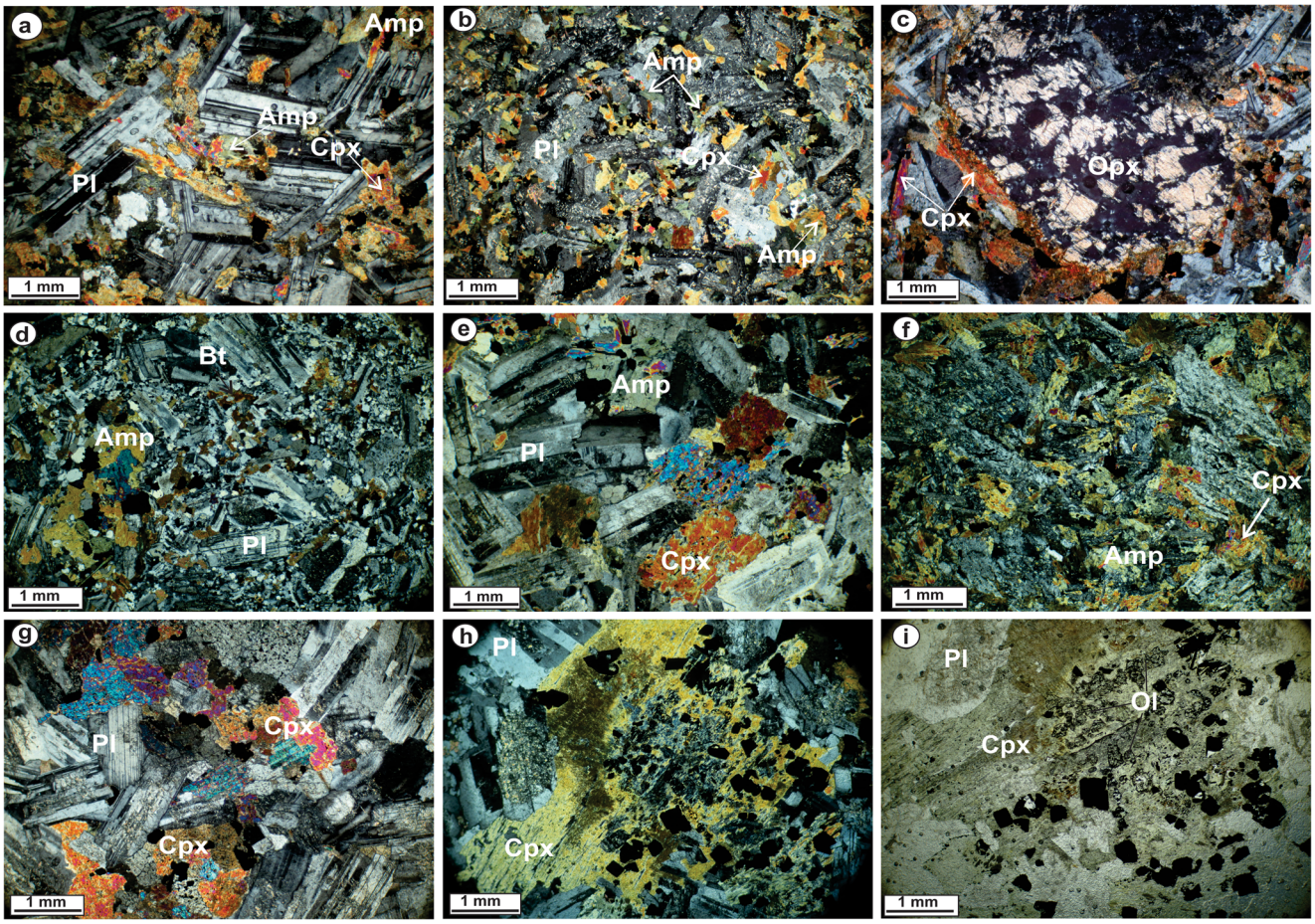

Fig. 2 Photomicrographs of the Kahak mafic-intermediate rocks. Abbreviations for mineral names after Whitney and Evan (2010): Pl = plagioclase; Cpx = clinopyroxene; Amp = amphibole; Bt = biotite; Opx = orthopyroxene

Cathodoluminescence (CL), reflected and transmitted light images were obtained. U-Pb dating and trace element analyses of the zircons were conducted synchronously by laser ablation-inductively coupled plasma-mass spectrometry (*LA-ICP-MS*) (Table S1 and Table S2 in ESM). Laser sampling was performed using a GeoLas 2005 and an Agilent 7500a ICP-MS instrument was used to acquire ion signal intensities. The diameters of the laser ablation craters were 32 μm. Zircon 91,500 was used as external standard for U-Pb dating and was analyzed twice every five analyses. Detailed operating conditions for the laser ablation system and the ICP-MS instrument and data reduction are the same as described by Liu et al. (2008, 2010a, 2010b). Offline selection and integration of background and analytical signals, time-drift correction, quantitative calibration for trace element analyses and U-Pb dating were performed by ICP-MS Data Cal (Liu et al. 2008, 2010b). Concordia diagrams and weighted mean calculations were made using Isoplot ver3 (Ludwig 2003).

Chemical analysis

The samples were coated with carbon prior to analysis. The precautions suggested by Zhang and Yang (2016) were applied to minimize the difference of carbon film thickness among samples and obtain a ca. 20 nm uniform coat. Mineral compositions were determined with a JEOL JXA-8100 electron probe micro-analyser (EPMA) equipped with four wavelength-dispersive spectrometers (WDS). During the analysis, an accelerating voltage of 15 KV and a beam current of 20 nA were used, and the electron beam was focused to a 10 μm spot. The peak counting time was 10 s for Na, Mg, Al, Si, K, Ca, Fe and 20 s for Mn and Ti. The background counting time was one-half of the peaks counting time on the high- and low energy background positions. For all elements the Kα lines were analyzed. The following reference materials were used: jadeite (Na), olivine (Si), pyrope garnet (Al, Fe), diopside (Ca, Mg), sanidine (K) and rutile (Ti). Data were corrected on-line using a ZAF (atomic number, absorption, fluorescence) correction procedure.

Whole-rock samples were crushed in a corundum jaw crusher (to 60 mesh). About 100 g were powdered in a tungsten carbide ball mill to less than 200 mesh. Major and trace element analyses of the samples pulverized by the tungsten carbide mill exhibited insignificant contamination from the mortars and the mills. The tungsten carbide mill contaminated samples with tungsten and cobalt only (Yamasaki 2018; Zhang et al. 2007; Takamasa and Ichinakai 2009). Tungsten and Co data were not used in the present study.

X-ray fluorescence (XRF) analyses of major element concentrations were performed on fused glass disks with a Rigaku ZSX Primus II spectrometer (Table 1); the operating conditions were 50 kV and 50 mA. Lithium borate flux was used to prepare glass disks, using a Katanax K1 Prime furnace. Based on repeated analyses of international reference materials, uncertainties for XRF analyses are ±1% relative for concentrations above 0.2%. The analytical precisions for major elements were better than 0.01% estimated from repeated analysis of the standards LAT-CS9, ncsdc73303, SARM-3, SARM-32 and SARM-45. To measure loss on ignition (LOI), each sample was dried at 105 °C, followed by calcination at 1000 °C in a muffle furnace for 4 h.

For trace element analyses, the whole rocks were dissolved by HF + HNO_3 in Teflon bombs and analyzed with an Agilent 7200a ICP-MS. During the determination, AGV-2, BHVO-2, BCR-2 and RGM-2 are used as reference materials. Rh was used as an internal standard to monitor signal drift during counting in inductively coupled plasma *mass spectrometry* (ICP-MS) analysis. The USGS rock standards GSP-1 were chosen for calibrating element concentrations of measured samples. Detailed sample digestion procedures for ICP-MS analyses and analytical precision and accuracy for trace elements are similar to those described by Liu et al. (2008).

Sr-Nd-Pb isotope analysis

Whole-rock Sr-Nd-Pb isotopic compositions were measured using a Finnegan Triton TI TIMS (Table 2), following the procedures of Pu et al. (2004, 2005). For Sr-Nd isotope determination, about 50 mg samples were dissolved in the same manner as for trace element analyses. Complete separation of Sr was achieved by a combination of cation exchange chromatography in H+ form and pyridinium form with the DCTA. Nd was then separated from the REE fractions by cation-exchange resin using HIBA as eluent. After purification, the separated Sr was dissolved in 1 μL of 1 NHCl and then loaded with TaF5 solution onto W filaments for TIMS analysis. The separated Nd was dissolved in 1 μL of 1 NHCl and then loaded with H_3PO_4 solution onto Re double-filaments. The mass fractionation corrections for $^{87}Sr/^{86}Sr$ and $^{143}Nd/^{144}Nd$ ratios were based on 86Sr/88Sr = 0.1194 and $^{146}Nd/^{144}$ Nd = 0.7219, respectively. During the laboratory analysis, measurements of NIST SRM-987 Sr standard yielded $^{87}Sr/^{86}Sr$ ratio of 0.710262 ± 0.000007 (2σ), and the JNdi-1 Nd standard yielded $^{143}Nd/^{144}Nd$ ratio of 0.512111 ± 0.000005 (2σ), similar to the reported data of 0.512115 ± 0.000007 by Tanaka et al. (2000). Total analytical blanks were 5 × 10–11 g for Sm and Nd, and (2 ~ 5) × 10–10 g for Rb and Sr.

For Pb isotope ratio determination, about 50 mg samples were completely dissolved in teflon vials with HF + HNO_3 and Pb were subsequently separated using anion-exchange columns with diluted HBr as an eluent. Analytical reproducibility of 0.01% (2σ) for $^{206}Pb/^{204}Pb$, 0.01% for $^{207}Pb/^{204}$ Pb, and 0.02% for $^{208}Pb/^{204}$166 Pb were attained in this study. Mass fractionation corrections have been made from runs of the NBS-981 standard based on the reported value of Todt et al. (1996), and the error on the mass fractionation corrections is 0.04%. Measured values for the NBS-981 Pb isotope standard yielded 16.9350 ± 0.0006 for $^{206}Pb/^{204}Pb$, 15.4836 ± 0.0006 for $^{207}Pb/^{204}$ Pb and 36.6799 ± 0.0016 for $^{208}Pb/^{204}$ Pb.

Results

Petrography

The Naragh gabbro-diorite, Kerogan gabbro, Veshnaveh quartz diorite, Fordou hornblende gabbro, and Bidhand gabbro are discussed in order of age based on U-Pb ages and geochemical correlations. The Bidhand intrusion has no radiometric ages. However, based on the geochemical similarities of Bidhand samples to the Miocene Kerogan and Fordou intrusions, Bidhand is assumed to also have a Miocene age.

Naragh gabbroic to diorite sills (Eocene) have granular textures; most are coarse (Fig. 2a) or fine (Fig. 2b) grained but some have bimodal or seriate textures. The major rock-forming minerals are plagioclase and clinopyroxene. Rare orthopyroxene crystals rimmed by clinopyroxene are present (Fig. 2c). Amphibole typically occurs as small, late stage crystals or as rims on clinopyroxene. One Naragh (i.e., TS8) has a unique mineralogy with fine to medium grained plagioclase and amphibole (Fig. 2b). The amphibole in this sample, which is similar in composition to the other sills, might indicate a higher volatile content in the magma from which it formed.

The Veshnaveh quartz diorite intrusion (Eocene) was emplaced in tuffs and andesitic lava south of Veshnaveh (Fig. 1). It was in turn intruded by a felsic pluton and multiple aplite dikes cut the quartz diorite. The quartz diorites have inequigranular textures and are comprised of plagioclase and minor amounts of biotite and amphibole (Fig. 2d). The accessory minerals are zircon, titanite, and Fe-Ti oxides.

The Kerogan gabbros (Miocene) are coarse grained, consisting of compositionally zoned plagioclase and clinopyroxene that has been partly modified to amphibole (Fig. 2e). Increasing water content of magma in the course

Table 1 Chemical compositions of the Kahak mafic-intermediate intrusive rocks

Sample	Eocene				Miocene					Miocene (based on stratigraphy)		
	Group 1				Group 2							
	Vesnaveh		Naragh		Kerogan			Fordou		Bidhand		
	VS22	VSA21	TS8	NA5	KRA31	KR32	KR31	KH29	KH9	KA12	KA5	KA18
Major oxides (wt%)												
SiO_2	57.8	58.2	51.4	52.3	50.9	50.3	53.2	49.8	50.4	51.0	49.5	47.7
TiO_2	0.8	0.8	1.3	1.6	0.8	1.1	0.6	0.9	0.9	0.8	0.9	1.6
Al_2O_3	18.2	18.5	16.8	16.0	19.4	18.4	22.7	21.7	21.9	21.3	18.8	15.3
FeOt	9	8.9	11.3	12.1	9.3	11.1	6.1	8	8.3	4.3	11.1	11.4
MnO	0.1	0.1	0.2	0.2	0.1	0.1	0.1	0.1	0.2	0.1	0.1	0.2
MgO	2	2	4.9	4.4	5.4	4.5	2.1	2.5	2.7	3.6	5.2	7.1
CaO	6.2	6.3	8.7	9.0	9.2	10.1	8	9.7	9.3	12.9	6.3	10.8
Na_2O	3.9	3.7	3.1	3.2	4.1	3.7	4.5	3.8	3.8	3.3	4.7	3.6
K_2O	1.1	1.1	0.8	1.2	0.2	0.3	0.9	1.0	1.0	0.8	1.2	0.6
P_2O_5	0.2	0.2	0.2	0.3	0.1	0.1	0.1	0.1	0.1	0	0.1	0
LOI	0.6	0.9	1.2	0.8	1.0	1.8	1.6	1.7	1.6	1.5	4.6	6.2
Total	99.6	99.7	98.6	100.2	99.6	98.1	98.2	99.6	98.5	98.2	97.9	98.2
Mg#	28.8	28.7	43.4	39.2	50.9	42	38	35.7	36.6	59.3	45.7	52.4
A/CNK	1	1	0.8	0.7	0.8	0.7	1	0.9	0.9	0.7	0.9	0.6
K_2O/Na_2O	0.3	0.3	0.3	0.4	0.1	0.1	0.2	0.3	0.3	0.2	0.3	0.2
K_2O+Na_2O	5	4.8	3.8	4.3	4.3	4.0	5.3	4.7	n.a.	4.1	6	4.2
K_2O+Na_2O-CaO	−1.2	−1.6	−4.9	−4.7	−4.9	−6.1	−2.7	−5	n.a.	−8.8	−0.3	−6.6
Trace elements (ppm)												
Ba	208	196	204	329	123	180	259	199.5	210	636	168	111
Cs	0.4	0.3	0.3	1.2	0.1	0.3	0.4	1.1	n.a.	1.4	0.9	0.4
Ga	16.9	16	19.1	18	17.1	16.8	17	16.6	16	19.1	17	16
Hf	3.9	3.9	3.4	4.3	1.5	1.8	1.2	1.7	n.a.	1.1	1.4	2.8
Nb	5.9	6	7.1	8	2.2	2.5	3	2.6	3	1.5	3	5
Rb	24.8	23	17.1	30	4	17.6	22	28.6	27	17	26	13
Sn	1	1.2	2	2	1	1	1	1	n.a.	<1	1.0	1
Sr	384	345	386	313	338	393	523	495	478	446	285	275
Ta	0.4	0.4	0.6	0.5	0.1	0.2	0.2	0.2	n.a.	0.1	0.1	0.2
Th	2.4	2.3	3.2	3.9	1.1	1.4	1.7	0.7	n.a.	0.3	1.0	0.6
U	0.8	0.9	0.9	1.1	0.1	0.4	0.5	0.3	n.a.	0.2	0.3	0.3
V	120	100	292	399	283	409	103	168	n.a.	211	341	224
W	1	n.a.	1	2.0	<1	1	1	5	n.a.	4	<1	1
Zr	140	121	126	143	49	62	26	58	45	33	48	92
Y	26.4	24	30.4	37	18.6	18.7	15	19.4	19	16.4	19	25
Cr	10	9	90	63	30	20	7	70	5	70	16.0	55
Ni	n.a.	3	20	17	14	7	2	n.a.	1	3	18	21
La	14.5	13.2	15	18.5	5	5.4	8	5.2	n.a.	3.7	6.3	5.3
Ce	34.7	32	33.7	40.1	13.5	13.7	17.2	15.3	n.a.	9.1	13.6	12
Pr	4.3	4	4	5.2	2	1.8	2.2	2.2	n.a.	1.2	1.8	1.7
Nd	19	15	17.2	23	9.1	8.5	1.0	9.1	n.a.	5.3	8	9
Sm	5.2	4.9	4.4	6	2.6	2.5	2.4	2.6	n.a.	1.8	2.4	2.8
Eu	1.3	1.2	1.2	1.6	0.9	0.9	1	1.1	n.a.	0.8	0.8	1
Gd	4.8	4.7	4.7	6	3	2.9	2.6	2.9	n.a.	2.2	2.7	3.5
Tb	0.8	0.8	0.8	1	0.5	0.5	0.4	0.5	n.a.	0.4	0.5	0.6

Table 1 (continued)

Sample	Eocene				Miocene					Miocene (based on stratigraphy)		
	Group 1				Group 2							
	Vesnaveh		Naragh		Kerogan			Fordou		Bidhand		
	VS22	VSA21	TS8	NA5	KRA31	KR32	KR31	KH29	KH9	KA12	KA5	KA18
Dy	4.5	4	4.8	6	3	3	2.6	3.2	n.a.	2.7	3	3.8
Ho	1	0.9	1	1.3	0.7	0.6	0.6	0.7	n.a.	0.6	0.7	0.8
Er	2.7	2.7	3	3.5	1.9	1.9	1.5	2.0	n.a.	1.7	1.9	2.4
Tm	0	0	0.4	0.5	0	0.3	0.3	0.3	n.a.	0.3	0.3	0.4
Yb	2.8	2.7	2.8	3.5	2	1.8	1.5	2.1	n.a.	1.8	1.9	2.7
Lu	0.4	0.5	0.5	0.6	0.3	0.3	0.2	0.3	n.a.	0.3	0.3	0.4
Pb	n.a.	2	2	5	1	1	3	n.a.	6	2	2	3
Eu/Eu*	0.8	0.8	0.8	0.8	1	1	1.2	1.2	n.a.	1.3	1	1
Sum-REE	96	86.6	93.5	116.8	44.5	44	50.5	47.5	n.a.	31.8	44.2	46.3

Note:

FeOt: *total iron oxide*

LOI: loss on ignition

A/CNK: Al_2O_3 / (CaO + Na_2O + K_2O) (molar ratio)

Eu*: Eu/Eu* = ((Sm_N + Gd_N) × 0.5). Normalizing values are after Boynton (1984)

n.a: not analyzed

of fractionation is likely to have contributed to amphibole stability, which crystallized on the clinopyroxene rims.

The gabbro east of Fordou (Miocene), intrudes basalt and basaltic-andesite lava (unit E6 on the map in Fig. 1). The Fordou gabbro mainly exhibits granular textures. The main constituent minerals are plagioclase and clinopyroxene. Large clinopyroxene crystals poikilitically encloses relicts of olivine and orthopyroxene (Fig. 2f, g); they were partially converted to chlorite and amphibole during hydrothermal alteration of the pluton.

The Bidhand gabbro (Miocene?), with an outcrop area of ~3 km^2, intruded the volcanic rocks of unit E6 in northwestern part of study area (Fig. 1b). Contacts between the gabbro and volcanic rocks are sharp. Gabbroic rocks from Bidhand are medium-grained, equigranular, and mostly composed of plagioclase and clinopyroxene (Fig. 2h). A few coarse-grained gabbroic intrusions are present that have sharp contacts with the host, finer grained gabbro. A few Bidhand gabbros show transition from plagioclase + clinopyroxene to plagioclase + amphibole mineral assemblage (Fig. 2i). Presence of varying amounts of amphibole in the mineral assemblages probably implies varying H_2O contents of the melts. Based on the whole-rock geochemical similarities of Bidhand gabbros to the Kerogan and Fordou intrusions, the Bidhand rocks are assumed to have Miocene ages.

LA-ICP-MS zircon U-Pb dating and trace element data

General remarks

Zircon U-Pb isotope and trace element data for 5 samples from the mafic-intermediate rocks are listed in Tables S1 and S2 in the

Table 2 Sr–Nd-Pb isotopic compositions for plutonic mafic-intermediate rocks from Kahak, Iran

Sample	Age (Ma)	($^{87}Sr/^{86}Sr$)i	εNd(t)	$^{87}Sr/^{86}Sr$	$^{143}Nd/^{144}Nd$	$^{143}Nd/^{144}Ndi$	T_{DM}	$^{206}Pb/^{204}Pb$	$^{207}Pb/^{204}Pb$	$^{208}Pb/^{204}Pb$	U (ppm)	Pb (ppm)	Th (ppm)
NA5	45	0.7054	1.4271	0.7055	0.5127	0.5127	0.98	18.59	15.63	38.72	1.12	5	3.91
KH29	20	0.7054	6.2611	0.7055	0.5130	0.5129	0.37	18.58	15.64	38.65	0.33	6	0.66
KRA31	21.5	0.7053	4.2928	0.7053	0.5129	0.5128	0.77	n.a.	n.a.	n.a.	0.10	1	1.06
VS22	51.7	0.7047	3.2446	0.7049	0.5128	0.5127	0.79	18.68	15.65	38.78	0.80	2	2.35
KR31	21.9	0.7055	3.4447	0.7056	0.5128	0.5128	0.61	18.72	15.66	38.82	0.49	3	1.73
KA5	44	0.7061	2.1556	0.7063	0.5127	0.5127	1.67	18.52	15.63	38.61	0.28	2	1.01
KR32	22	0.7053	4.2014	0.7053	0.5127	0.5128	0.90	18.70	15.65	38.81	0.40	1	1.36

electronic supplementary material (ESM) respectively. Zircon grains have typical oscillatory magmatic zoning without inclusions.

The zircons have two distinct rare earth elements (REE) patterns (Figs. 3a–e and 4a, c) and the majorities of zircons have moderate negative Eu anomalies, positive Ce anomalies, and significant depletions in La and enriched patterns for heavy rare earth elements (HREE). These zircons are considered to be magmatic (Belousova et al. 2002). REE partition coefficients calculated for zircons from Kahak intrusive rocks are comparable with zircons partition coefficients for magmatic rocks (Hanchar and van

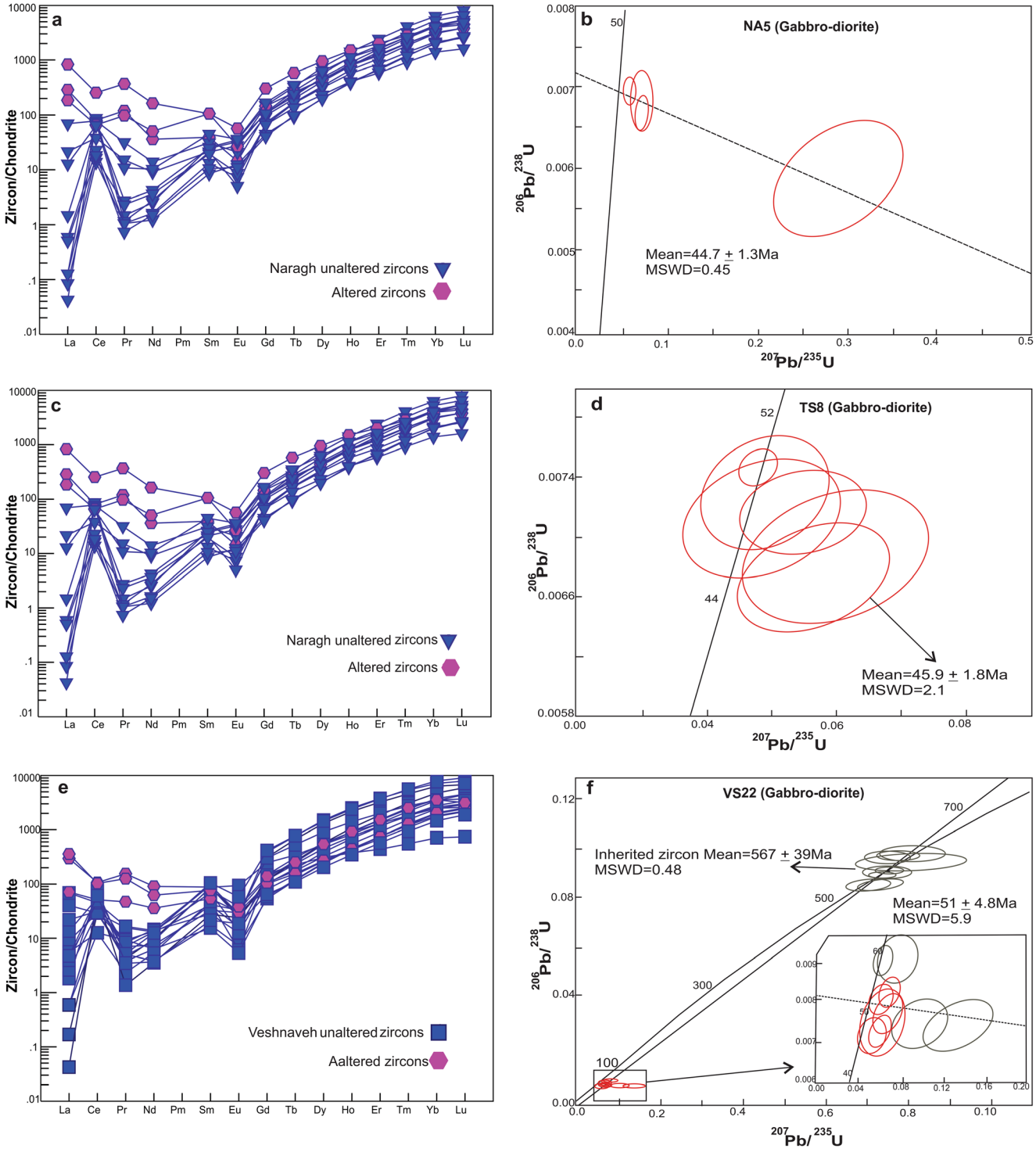

Fig. 3 **a**, **c**, **e** Chondrite-normalized trace-element patterns of the zircons for Eocene rocks from the Kahak area. The normalizing values are from Sun and McDonough (1989). Two types of zircon are shown with different colors. **b**, **d**, **f** U-Pb concordia diagrams of the zircons

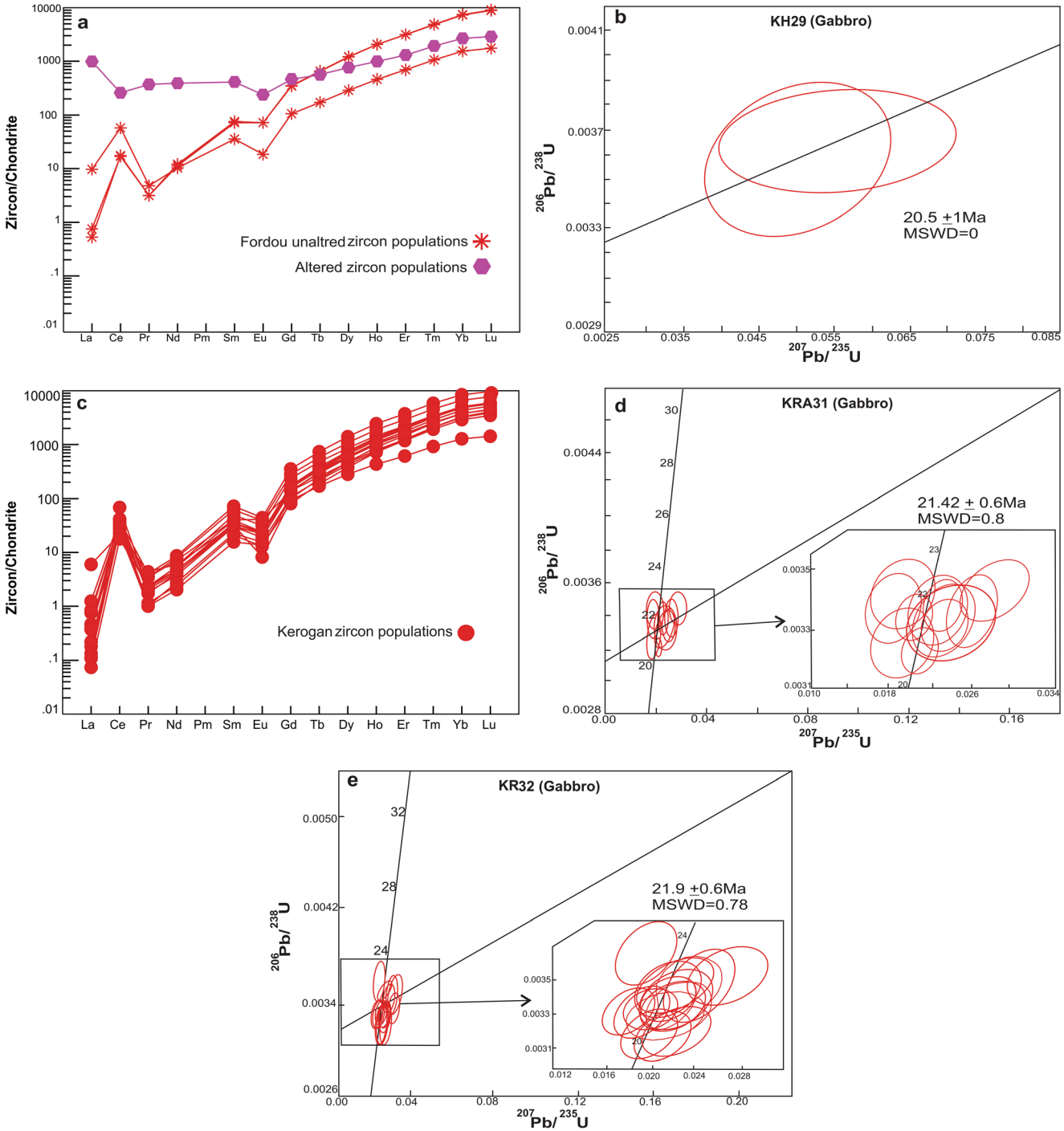

Fig. 4 **a**, **c** Chondrite-normalized trace-element patterns of the zircons for Miocene rocks from the Kahak area. The normalizing values are from Sun and McDonough (1989). Two types of zircon are shown with different colors. **b**, **d**, **e** U-Pb concordia diagrams of the zircons. Trace-element data of the zircons from sample KR32 are not available

Westrenen 2007). However, a few zircon grains have elevated light rare earth elements (LREE) abundances with only slight positive Ce anomalies and negative Eu anomalies (Figs. 3a, c and 4c); these characteristics imply some zircon crystallized in the presence of aqueous fluid at the end of magmatic evolution (Hoskin and Schaltegger 2003).

The majority of zircons in Kahak mafic rocks are magmatic zircons, presenting crystallization ages of their host rocks. Zircons from three age dated samples (i.e., NA5, TS8 and VS22) show wide, almost continuous age ranges of 37.7–53.3, 37.9–52.3 and 46.5–53.0 Ma (1σ) respectively. These comprise 7–16 Myr time intervals. For these three

samples, the weighted mean ages are considered as the magmatic ages. However, zircons age dated in three samples (i.e., KRA31, KR32 and KH9) show restricted magmatic age ranges from 20.4 to 23.5 Ma (1σ).

Kahak intrusive rocks also contain some older zircons which are regarded as inherited zircons. These can be classified into two groups; group one (G1) is older than 533 Ma and group two (G2) is of Cenozoic age but slightly older than the magmatic ages of their host rocks. G1 inherited zircons are derived from basement crustal rocks which have been assimilated by ascending magmas. G2 inherited zircons are derived from older, coeval magmatic rocks. Four age dated samples are almost devoid of G1 inherited zircons (i.e., NA5, TS8 and KR32 lack inherited zircons and KRA31 only include one inherited zircons), whereas samples KH9 and VS22 include two and eight G1 inherited zircons respectively. Three of the age dated samples from the study area (i.e., VS22, KR32, and KRA31) contain a few G2 inherited zircons (see below).

Naragh gabbro-diorite (Eocene)

Zircon grains from sample NA5 are euhedral to subhedral and most are 50–110 μm long with oscillatory zoning, indicating magmatic origins (Hoskin and Schaltegger 2003; Wu and Zheng 2004). The $^{206}Pb/^{238}U$ ages include a rather continuous range from 37.7 to 53.3 Ma for 11 spots. A weighted mean age of 44.7 ± 1.3 Ma (1σ), (MSWD = 0.45) is considered to be the crystallization age of this gabbroic sill (Fig. 3a).

The zircon grains in sample TS8 are subhedral to euhedral and 60 to 110 μm in length with most showing concentric zoning. Eleven spots yielded a continuous range of ages from 37.9 to 52.3 Ma. They yield a weighted mean $^{206}Pb/^{238}U$ age of 45.9 ± 1.8 Ma (1σ), (MSWD = 2.1, Fig. 3d), which is, within uncertainty, the same age as zircon in sample NA5. We take this to be the best estimate of the crystallization age for this Naragh gabbro-diorite sill.

Samples NA5 and TS8 also present a few younger ages for zircons, in the former, three spots are 26.6 27.9 and 30.9 Ma, and in the latter, four spots have ages from 20.4 to 27.9 Ma. These might be explained by sampling from the contact with younger gabbroic dykes. Gabbroic dykes which are down to cm size in thickness (Gill 2010; p. 95) particularly those having similar mineralogy and texture with the host/country rocks are likely to have been unnoticed in the study area.

Veshnaveh diorite (Eocene)

Zircon grains from quartz diorite sample (VS22) are subhedral to euhedral and most are of 50–100 μm long. Nine spots have a continuous range of $^{206}Pb/^{238}U$ ages from 46.5 to 53.4 Ma. The weighted mean age of these spots is 51 ± 4.8 Ma (1σ) which is considered to be the age of the magmatic event that produced Veshnaveh diorites (Fig. 3f). Eight spots have $^{206}Pb/^{238}U$ ages ranging from 533.0 to 670.9 Ma and two spots have 58.7 and 59.0 Ma ages; these are considered as G1 and G2 inherited zircons respectively (G1 is inherited from basement crustal rocks and G2 from older, coeval magmatic rocks).

Kerogan gabbro (Miocene)

Most zircon grains from samples KR32 and KRA31 are 50–150 μm long. They are euhedral to subhedral and show oscillatory growth zoning in CL images, suggesting a magmatic origin. Twenty-one spots were analyzed in sample KR32, of which 17 spots yielded concordant $^{206}Pb/^{238}U$ ages ranging from 20.4 to 23.5 Ma with a weighted mean of 21.9 ± 0.6 Ma (1σ) (MSWD = 0.78), (Fig. 4e). In sample KRA31, thirteen zircon grains yielded a mean age of 21.4 ± 0.6 Ma (1σ) (MSWD = 0.87). We interpret these ages to mark magma crystallization (Fig. 4d).

Sample KR32 contains two spot analyses of zircon with 29.0 and 37.0 Ma ages. Sample KRA31 contains one spot analysis of zircon with 27.1 Ma age. These are considered as zircons inherited from older, coeval magmatic rocks (G2 inherited zircons).

Fordou gabbro (Miocene)

The Fordou gabbro (KH 29) yielded only 4 zircon grains, two of which had a mean age of 20.5 ± 1.0 Ma (1σ), and this is considered to be the age of intrusion (Fig. 4b). The other two zircons appear to have been inherited from basement crustal rocks (G1 inherited zircons).

Mineral chemistry

Clinopyroxenes in the gabbros and gabbroic diorite are mainly augite but some clinopyroxenes fall in the diopside field (Fig. 5a). Plagioclase compositions range widely, with some sodic compositions the result of minor alteration. In the Eocene Naragh gabbros and diorites plagioclases are $An_{44–56}$ and for the Miocene Kerogan they are $An_{6–70}$ (Fig. 5b). On the $Mg/(Mg + Fe^{2+})$ versus T_{Si} (Si atoms per formula unit) diagram (Leake et al. 1997), amphiboles from the Eocene Naragh gabbro-diorites are mostly actinolite and those from the Miocene Kerogan gabbro vary from actinolite to magnesio-hornblende. The actinolitic compositions indicate some of the amphiboles are secondary (Fig. 5c).

Whole rock major and trace element geochemistry

On the R1 vs R2 diagram for plutonic rocks (Fig. 6a), the Kahak mafic-intermediate samples plot in gabbro, gabbroic-diorite, and diorite fields with the Eocene rocks having higher R1 values. In the total alkali-silica (TAS) diagram

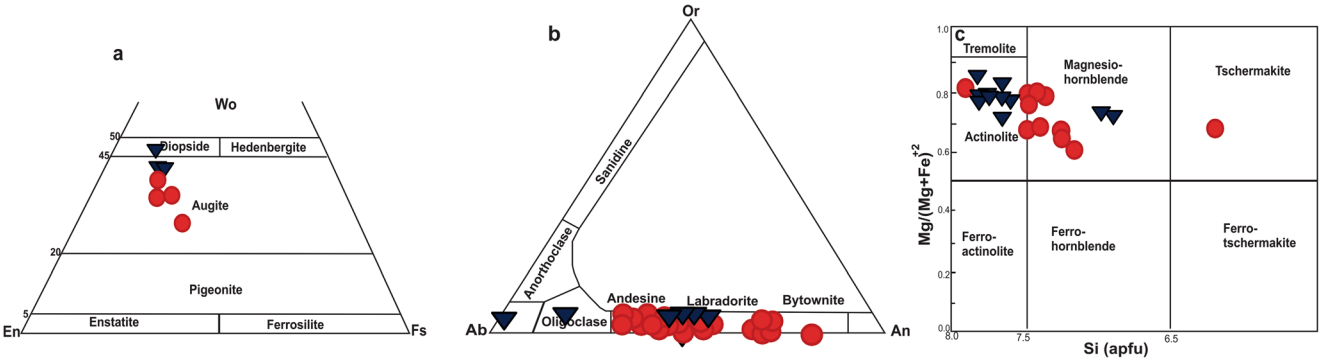

Fig. 5 Mineral compositions of Eocene Naragh (closed triangles) and Miocene Kerogan (closed circles) mafic-intermediate rocks depicted on classification diagrams. **a** Clinopyroxenes are augite and subcalcic augite (Morimoto 1988). **b** Plagioclases are mostly labradorite and andesine (Deer et al. 1991) with two analyses that are more sodic and probably secondary. **c** Amphiboles are mostly in the actinolite to magnesio-hornblende domains on the Mg/(Mg + Fe) versus total Si diagram of Leake et al. (1997)

(Middlemost 1994), the samples are gabbro, gabbroic diorite, and diorite with one sample from the Fordou pluton in the monzodiorite field (Fig. 6b). The mafic rocks are all metaluminous with A/CNK ratios of 0.6–0.9. Kahak intrusive rocks have high Fe/Mg ratios revealing tholeiitic (or ferroan) characteristics using Miyashiro's (1974) criterion (Fig. 6c). However, on an AFM diagram, they plot on the boundary between calc-alkaline and tholeiitic fields (Fig. 6d).

The U-Pb ages clearly indicate that there was an approximately 25 Myr gap between Eocene and Miocene magmatisms in this part of the UDMA, thus, it is likely that these magmatisms were originated from different source regions and evolved under different conditions. So one might question plotting both groups of intrusions (Eocene and Miocene rocks) on the same variation diagrams and interpreting their petrogenetic evolution based on the overall trends. Therefore, to highlight the geochemical

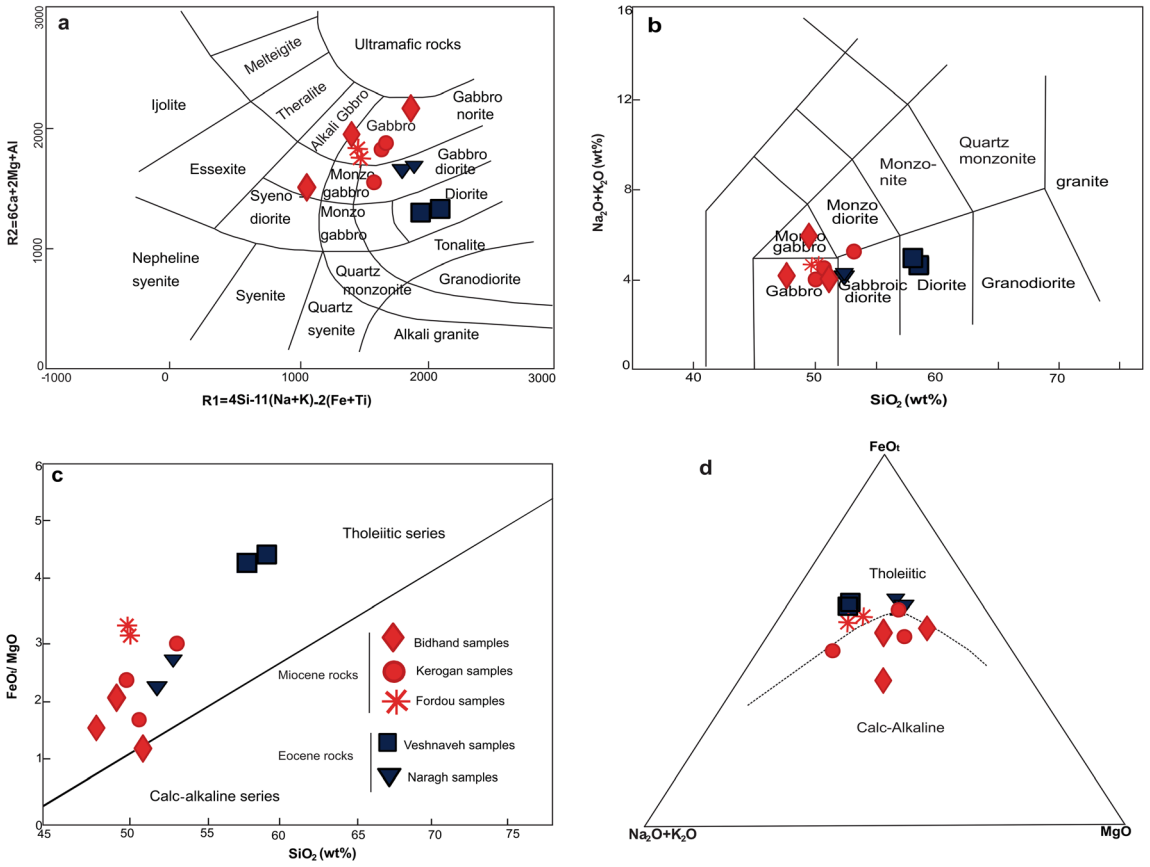

Fig. 6 Classification diagrams for the Kahak mafic-intermediate intrusive rocks. **a** R1 versus R2 diagram (de la Roche et al. 1980). **b** Total alkali versus silica (TAS) diagram (Middlemost 1994). **c** SiO_2 versus FeOt/MgO discrimination diagram (Miyashiro 1974). **d** AFM ($Na_2O + K_2O$-FeOt-MgO) plot (Irvine and Baragar 1971) for Kahak basic-intermediate rocks

differences between the Eocene and Miocene intrusions, the data for the Eocene rocks are marked by grey areas in Fig. 7. Compared at the same silica contents, the more tholeiitic Eocene suite is enriched in TiO_2 and FeOt and depleted in Al_2O_3 and Na_2O compared to the Miocene suite. The Eocene rocks also extend to higher silica contents. Normalized trace element patterns for the Kahak mafic-intermediate rocks also form two distinct groups; group 1 (Eocene) comprises incompatible trace-element rich intrusions (TERI, Fig. 8a, c) and, group 2 (Miocene) include incompatible trace-element poor intrusions (TEPI, Fig. 8b, d). The group 1 samples (the Eocene Naragh and Veshnaveh intrusions) have higher REE contents with slightly negative Eu anomalies (Fig. 8a). This Eocene group is more enriched in light rare earth elements)LREE(, Nb, and Ta and has higher La/Yb ratios (Fig. 8c) than the Miocene group (Fig. 8d). Except for the negative Nb-Ta-Ti anomalies and higher rare earth elements (HREE) contents, Eocene group 1 intrusions, have incompatible trace element concentrations intermediate between enriched mid-ocean ridge basalt)E-MORB(and OIB.

Group 2 gabbros (of Miocene age from the Kerogan and Fordou areas) are characterized by lower REE and other incompatible trace element abundances (Fig. 8b). These Miocene rocks also have strong negative Nb-Ta and strong positive Pb, K, Ba, Cs, and Sr anomalies (Fig. 8d). Slight negative to positive Eu anomalies, $(Eu/Eu^*)_N = 0.8–1.3$, in some of the Miocene gabbros are also notable (Fig. 8b).

Whole-rock Sr-Nd-Pb isotopes

The Sr and Nd isotopic ratios of the mafic Kahak intrusions are in the ranges of 0.7043–0.7060 and 0.5127–0.5130, respectively (Table 2). On a Sr-Nd isotopic diagram, the data plot close to the mantle array but slightly shifted towards higher $^{87}Sr/^{86}Sr_i$ for a given $\varepsilon Nd_{(t)}$ (Fig. 9a).

The more calc-alkaline Miocene rocks have slightly higher $(^{87}Sr/^{86}Sr)_i$ (0.7053–0.7061) and $\varepsilon Nd_{(t)}$ values (2.1–6.3) compared to their tholeiitic Eocene counterparts (0.7047–0.7054 and 1.4–3.2) and plot farther from the mantle array like typical arc magmatic rocks. The Kahak intrusions extend to lower $(^{87}Sr/^{86}Sr)_i$ and have higher $\varepsilon Nd_{(t)}$ than some other UDMA mafic-intermediate rocks (Fig. 9a), for instance from the Saveh area (Rezaei-Kahkhaei et al. 2011), the Niyasar area (Honarmand et al. 2014), the Kuhe-Dom area (Kananian et al. 2014), the Ardestan area (Babazadeh et al. 2017) and the Nain area (Yeganehfar et al. 2013). The $^{206}Pb/^{204}Pb$ $2^{07}Pb/^{204}Pb$, and $^{208}Pb/^{204}Pb$ ratios for the Eocene and Miocene Kahak rocks show overlap and range from 18.44 to 18.79, 15.59 to 15.83, and 38.51 to 39.37, respectively. These lead isotope ratios plot above the Northern Hemisphere Reference Line (NHRL; Hart 1984) and significantly higher than the Indian MORB. Significantly, the Pb-isotope ratios plot within the range of Indian Ocean marine sediments and of igneous rocks from the Java arc (Fig. 9b). They lie close to the enriched mantle component EMII.

Discussion

Alteration and element mobility

Petrography of the Kahak mafic-intermediate rocks reveals slight sericitization of plagioclase and chloritization of

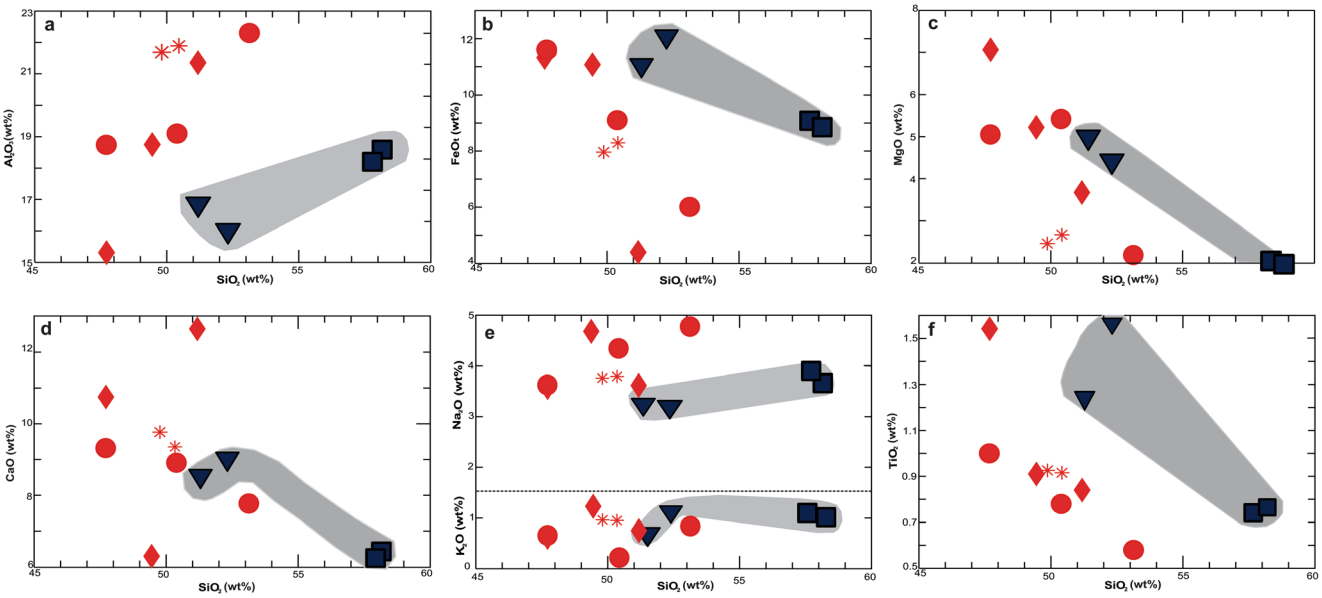

Fig. 7 SiO_2 versus major element oxides variation diagrams for the Kahak mafic-intermediate rocks. On some of the diagrams, the Eocene Veshnaveh and Naragh samples (shown by the grey area) plot in different areas and show distinct variation trends, as compared to the Miocene Kahak intrusions (red). Symbols as in Fig. 6

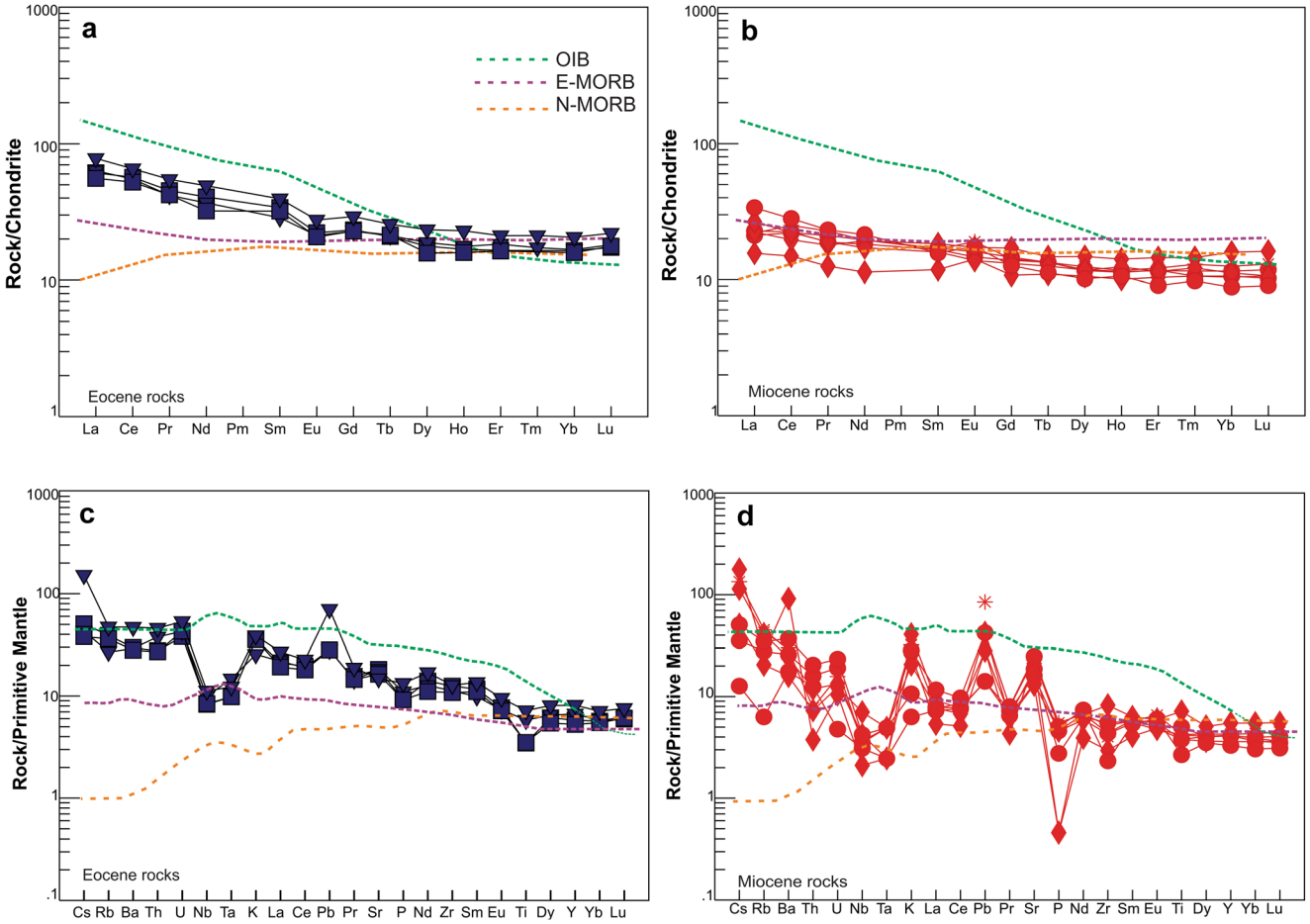

Fig. 8 **a**, **b** Chondrite-normalized rare earth element patterns for the incompatible element-rich Eocene Kahak intrusions (i.e., Veshnaveh and Naragh) and the incompatible element-poor Miocene Kahak intrusions (i.e., Kerogan, Fordou, Bidhand) respectively. Normalizing values are from Boynton (1984). **c**, **d** Primitive mantle normalized multi-element (spider) diagrams for the Kahak intrusions. Composition of OIB, MORB and the normalizing values are from Sun and McDonough (1989). Symbols as in Fig. 6

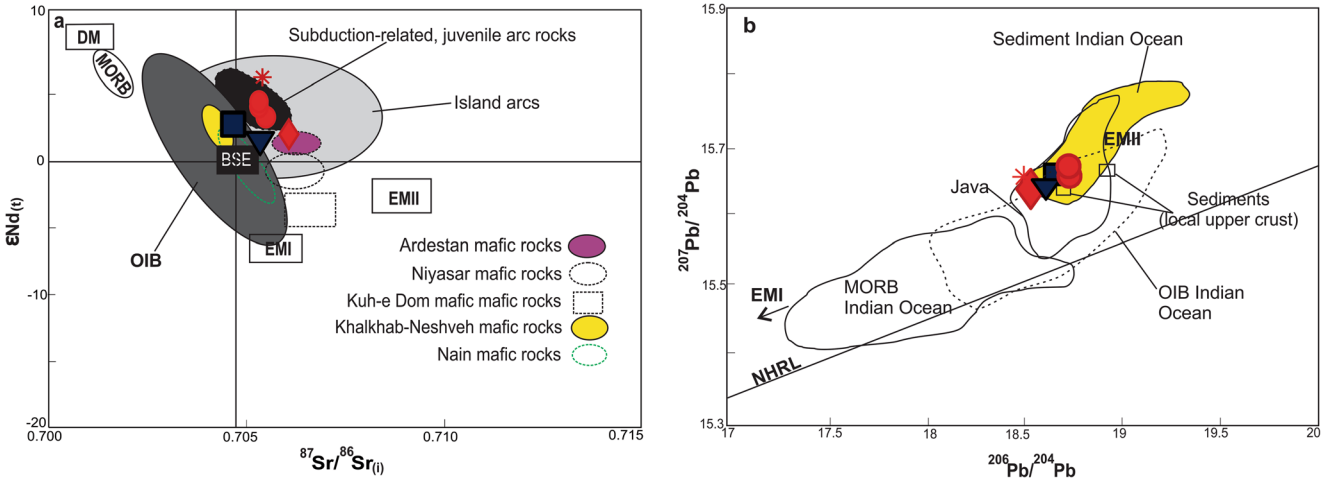

Fig. 9 **a** $(^{87}Sr/^{86}Sr)_i$ versus $\varepsilon Nd_{(t)}$ values for the Kahak mafic-intermediate intrusive rocks. DM, EMI, EMII and island arcs fields form Hart et al. (1986), subduction-related, juvenile magmas from Defant et al. (1992); OIB (White and Hofmann 1982; Hamelin et al. 1985); **b** $^{206}Pb/^{204}Pb$ versus $^{207}Pb/^{204}Pb$ diagram showing the composition of the Kahak intrusions. OIB, Indian Ocean (White and Hofmann 1982; Hamelin et al. 1985); Java (Whitford et al. 1981; Turner and Foden 2001); Sediments, Indian Ocean (Ben Othman et al. 1989); MORB, Indian Ocean (Dupré and Allègre 1983; Rehkämper and Hofmann 1997); the NHRL, Northern Hemisphere Reference Line (Hart 1984); Sediments from the local upper crust (Gertisser and Keller 2003). Symbols as in Fig. 6

ferromagnesian minerals, along with precipitation of secondary sodic plagioclase and actinolitic amphibole. However, most samples are largely unaltered.

The Kahak mafic-intermediate rocks were also assessed for secondary processes by plotting Zr (as a sensitive indicator of immobility) versus La, Nb, and Hf (Fig. S1 in the ESM). Nb, La, and Hf show broadly positive correlations with Zr suggesting that the geochemistry of the intrusive rocks was not significantly affected by post-emplacement alteration (e.g., Cann 1970; Polat and Hofmann 2003). Y/Ho ratios can also be used for evaluating the role of alteration. This ratio is 28 in fresh basaltic rocks (Bau 1996) and between 44 and 74 in altered rocks (Zhang et al. 1994; Bau et al. 1995). The Y/Ho ratios in the Kahak mafic-intermediate rocks range from 27 to 30, indicating that secondary processes were not significant.

Major element variation diagrams and normalized trace element patterns also preclude considerable alteration. The mafic to intermediate intrusions in the Kahak area have well-defined variation trends (Fig. 7) on major-element variation diagrams that distinguish the mafic plutonic rocks of Eocene age from those of Miocene age, particularly for TiO_2, Al_2O_3, and FeOt versus SiO_2. Moreover, the normalized trace element patterns of Kahak mafic-intermediate intrusions can also be classified into two distinct types (TERI and TEPI) that correlate with rocks of Eocene and Miocene age respectively. The distinctions are likely due to the modest differences in the evolutionary histories of their parent magmas.

Crustal contamination signatures

Different degrees of crustal contamination lead to the modification of major and trace element compositions and of radiogenic isotope ratios in mantle-derived magmas (e.g., Castillo et al. 1999; Wang et al. 2016). Continental crustal contamination of mafic magmas typically causes Ti and P depletion and enrichment of Th and LREEs (e.g., Taylor and McLennan 1995). Negative Ti anomalies are considered by some to be signatures of interaction with continental crust (Rudnick and Gao 2003). Except for slightly negative Ti anomalies in the Eocene Veshnaveh samples, the other Kahak mafic-intermediate rocks do not have large Ti troughs on primitive mantle-normalized multi-element diagrams (Fig. 8c, d).

Significant variation in large ion lithophile elements (LILE) such as K, Ba, Cs, and other highly incompatible elements such as Pb and Th, particularly in the Miocene samples, might be assigned to the effects of fractional crystallization or crustal contamination. Lower U-Th concentrations in the Miocene group 2 rocks point to a lack of significant crustal contamination (e.g., Plank 2005). Moreover, the narrow variation of Sr isotope ratios (0.7047–0.7061) and higher $\varepsilon Nd_{(t)}$ values (1.4 to 6.2) in the mafic Kahak rocks do not support significant contamination by old continental crust (Fig. 9a). The Kahak intrusive rocks have rather constant Nd isotopic ratios with increasing Sm/Nd ratio (Fig. 10a). This is consistent with fractional crystallization (or variable degrees of partial melting) and also implies that little or no crustal assimilation occurred during the crustal evolution of these magmas (Fig. 10a, b). However, based on 'process identification diagrams' that utilizes incompatible element ratios (i.e., highly incompatible element / incompatible element ratios), the Kahak mafic rocks seem to have experienced combined assimilation fractional crystallization (Fig. 10c). Contamination by older, coeval magmatic rocks is likely to have increased Sm/Nd, Rb/Zr and K_2O/Na_2O ratios but did not alter the isotopic ratios. Three of the age dated samples from the study area (i.e., VS22, KR32, and KRA31) contain zircons inherited from older, coeval magmatic rocks (i.e., G2 inherited zircon grains).

Although most of the mafic plutonic rocks lack zircons much older than the age of intrusion, some zircons in Eocene Veshnaveh diorite have Late Neoproterozoic to Early Cambrian (i.e., Ediacaran) ages. These are interpreted to be inherited zircons and the ages correlate with those of the basement rocks underlying the UDMA (Ramezani and Tucker 2003; Hassanzadeh et al. 2008). The absence or scarcity of G1 inherited zircons (i.e., zircons inherited from basement crustal rocks) in most of the Kahak mafic rocks also implies that the majority of magma batches have not experienced significant crustal contamination. Four out of six age dated samples (i.e., NA5, TS8, KR32 and KRA31) are almost devoid of G1 inherited zircons. Babazadeh et al. (2018) and Nouri et al. (2018) have reported inherited zircons in other magmatic rocks from the UDMA with rather high Sr and Nd isotope ratios (Fig. 9a); these led the authors to conclude that mafic parent magmas experienced moderate crustal contamination in the Ardestan and Saveh areas.

On the other hand $2^{07}Pb/^{204}Pb$ ratios of the Kahak rocks are higher than Indian MORB values and lie within the range of Indian Ocean marine sediments (Fig. 9b). Introduction of a small amount of subducted sediment into the mantle source of Kahak magmas might have led to significant change in Pb isotope ratios. We suggest that the Kahak mafic-intermediate plutons show isotopic characteristics of a depleted mantle source (MORB) which has been affected by subduction components. Moreover, the mantle source must have changed with time; Eocene gabbros and gabbroic diorites have less radiogenic Sr than do the Miocene gabbros which have more typical arc isotopic compositions.

Fractionation, accumulation and P-T of magma crystallization

Kahak mafic-intermediate rocks have low Mg# ([100 MgO/(MgO + FeOt)]; 29–59) and low compatible trace element contents (e.g., Cr and Ni). Therefore, they do not represent

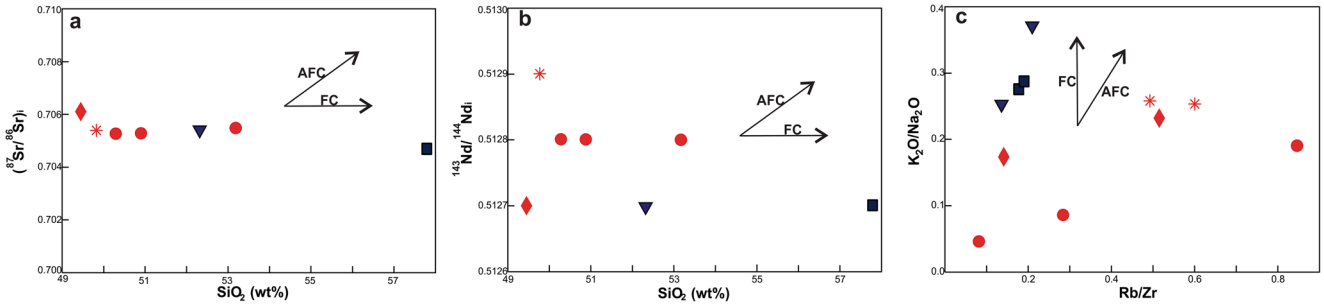

Fig. 10 Fractional crystallization (FC) and assimilation fractional crystallization (AFC) trends are shown on **a** $(^{143}Nd/^{144}Nd)_i$ versus Sm/Nd, **b** $(^{143}Nd/^{144}Nd)$ i versus SiO_2 and **c** K_2O/Na_2O versus Rb/Zr ratios plots for the mafic-intermediate rocks of the Kahak area. Symbols as in Fig. 6

primary magmas and they must have formed from magmas that experienced variable amounts of differentiation, particularly fractional crystallization within crustal magma chambers. For Miocene Kahak samples, decrease of CaO and increase of Al_2O_3 with increasing silica contents (Fig. 7) indicate that clinopyroxene fractionation played a major role in the evolution of the Miocene magmas from the Kahak area. Some lines of evidence support the accumulative nature of plagioclase in the Miocene Kahak rocks (i.e., Bidhand, Kerogan and Fordou intrusive rocks). Positive Sr and Eu anomalies are probably the most important consequence of feldspar accumulation. High Al and Na contents of the Miocene rocks further confirm the accumulation hypothesis. In contrast, the weakly negative Eu anomalies in the Eocene rocks (Fig. 8a) indicate feldspar removal during fractionation (Rollinson 1993). Higher silica and lower MgO contents of the Eocene Veshnaveh diorites as compared to the other intrusions from the Kahak area imply that they were formed from more differentiated melts.

The chemical composition of minerals such as clinopyroxene and amphibole are useful to estimate the physical conditions of magma crystallization. The compositions of pyroxene from the Kahak intrusive rocks are plotted in Al^{VI} versus Al^{IV} diagram of Aoki and Shiba (1993). Most of the studied samples plot in medium pressure field (Fig. S2a in the ESM). Soesoo (1997) also proposed the YPT versus XPT diagram to estimate the pressure and temperature of pyroxene crystallization.

The results suggest crystallization of the clinopyroxenes under 1100–1175 °C and 2 to 5 kb in the Naragh and Veshnaveh gabbros (Fig. S2b and c in the ESM). Variation of Al^{IV} and Ti values in calcic amphiboles (Fig. S2a in the ESM) can also be used to evaluate the crystallization history of magmas. Ti occupancy in amphibole depends strongly on temperature (Ernst and Liu 1998). Al_2O_3 contents increase with P and T. TiO_2 isopleths are strongly dependent on temperature but are nearly independent of P (Ernst and Liu 1998). Based on the Al_2O_3 and TiO_2 contents in amphiboles, the Kahak mafic-intermediate intrusions formed over a significant temperature range (650–950 °C), including subsolidus conditions (Fig. S2d in the ESM).

Source characteristics

The Kahak mafic-intermediate intrusive rocks, particularly the incompatible-element rich Eocene rocks, are arranged closed to and parallel with the mantle array on a Sr-Nd isotope plot (Fig. 9a).

The mantle affinity of the Kahak intrusive rocks is also confirmed by their normalized trace-element patterns which closely resemble mantle-derived melt end members (i.e., MORB, OIB, Figs. 8b, d). Nevertheless, variable degrees of LILE enrichment and high field strength elements (HFSE) depletion in the Kahak intrusions make them more similar to the partial melting products of subcontinental lithospheric mantle in magmatic arcs (i.e., subduction zones). REE patterns can reveal the nature of a mantle source, the extent of melting (George and Rogers 2002), and the equilibration depth (Tang et al. 2012) of magmas. The Kahak mafic-intermediate intrusive rocks have weakly fractionated chondrite-normalized REE patterns and rather elevated, flat HREE patterns with $(La/Yb)_N < 4$. All of these features and low Dy/Yb ratios (~2) suggest that their parent magmas last equilibrated in rather shallow mantle with a garnet-free, or only containing minor garnet, residue (Springer and Seck 1997), assuming the REE patterns did not charge during differentiation. Instead, the relatively flat M-HREE pattern of the Kahak rocks indicates a mainly spinel lherzolite mantle source. However, lower HREE abundances of the Miocene intrusions as compared to those of Eocene age indicate that the former was derived from a deeper source in the mantle. The Kahak mafic-intermediate magmas may have formed by 5–10% melting based on the La/Sm-Sm/Yb relations (Fig. 11a) outlined by Aldanmaz et al. (2000). Moreover, both suites plot in the spinel>garnet lherzolite field pointing to a greater role for spinel lherzolite relative to garnet lherzolite during partial melting (Fig. 11a).

Eocene tholeiitic gabbros similar to the Kahak mafic intrusives have also been recognized in the Eastern Pontides (Eyuboglu 2015) and Lesser Caucasus (Rezeau et al. 2017) along the Tethyan margin. The Kahak Eocene intrusives have rather enriched trace element patterns (i.e., similar to

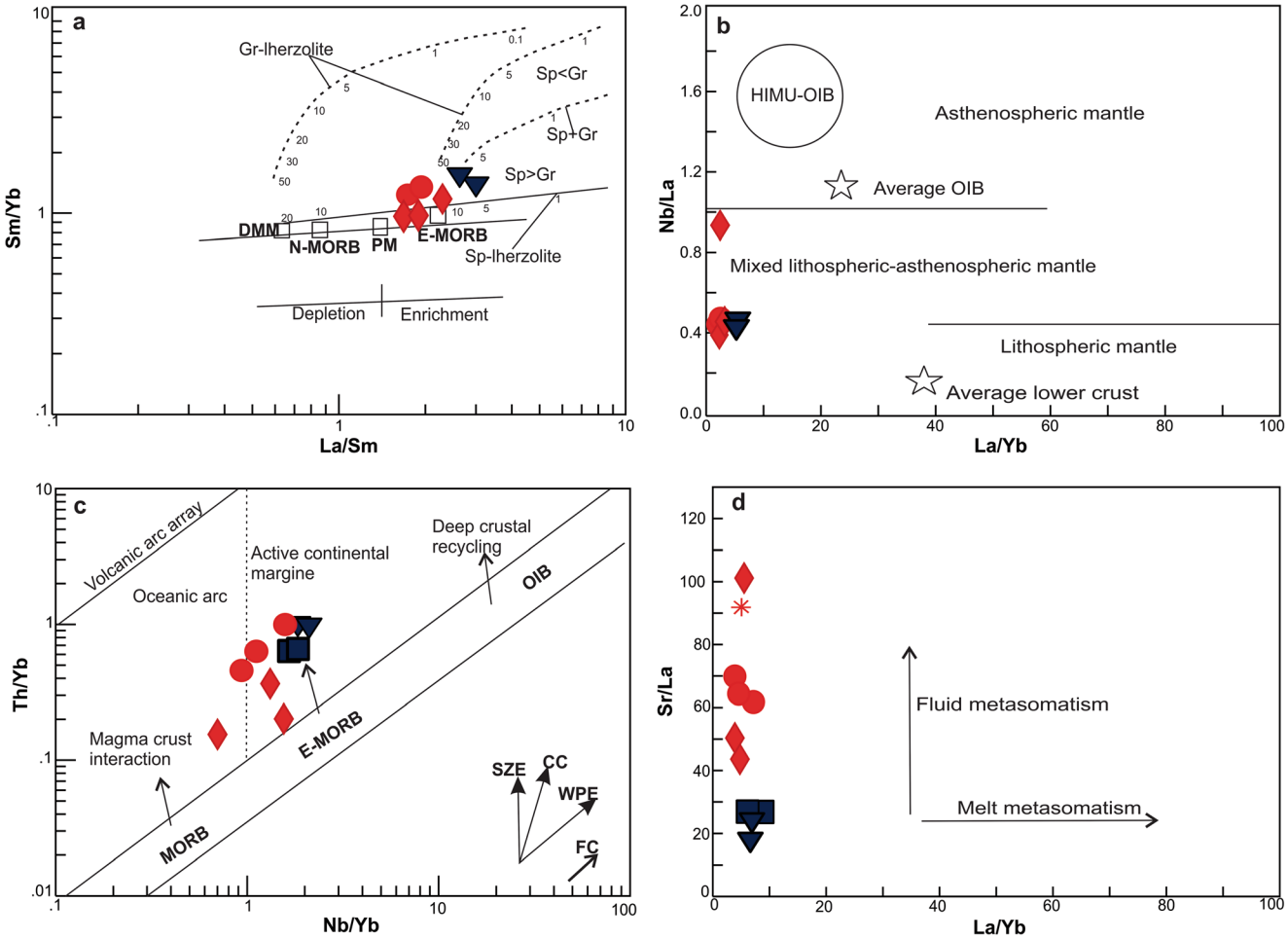

Fig. 11 Trace element variations in the Kahak intrusive rocks. To achieve the best result about the mantle source/s, five samples with MgO < 3.55 wt% are excluded (in diagrams **a** and **b**), with most samples having MgO > 4.5 wt%. **a** La/Sm versus Sm/Yb diagram for the Kahak intrusive rocks. Melting curves for garnet and spinel lherzolite are after Aldanmaz et al. (2000). Numbers along the curves represent the percent of partial melting for different proportions of garnet (Gt) and spinel (Sp). **b** Nb/La versus La/Yb variation diagram for the Kahak samples. The asthenospheric, lithospheric, and mixed mantle fields are after Smith et al. (1999). Average OIB, HIMU, and average lower crust are after Fitton et al. (1991), Smith et al. (1999), and Chen and Arculus (1995) respectively. **c** On a plot of Nb/Yb versus Th/Yb (Pearce 2008) all samples from the Kahak region plot above the MORB-OIB array. **d** Kahak intrusive rocks on a Sr/La vs La/Yb plot that distinguishes the effects of fluid metasomatism from melt metasomatism (Woodhead et al. 1998). Symbols as in Fig. 6

EMORB) whereas those in the Eastern Pontides have depleted trace element patterns (i.e., similar to NMORB). However, those in the Lesser Caucasus have a wide range of enriched to depleted trace element patterns. These variations in trace element patterns likely reflect the heterogeneous nature of the mantle wedge (including the subcontinental mantle) above a subducting slab of oceanic lithosphere. Geochemical characteristics of the Miocene Kahak intrusions resemble the Miocene calc-alkaline mafic plutonic rocks in the Ardestan area (Babazadeh et al. 2017), the 26 Ma basaltic rocks in the Nain area (Yeganehfar et al. 2013), and the mafic-intermediate rocks in the Niyasar area (Honarmand et al. 2014) of the UDMA (Fig. 9a), all of which were considered to have formed in an active continental margin environment.

Low Nb/La and La/Yb ratios (Nb/La <0.5 according to Smith et al. 1999) (Fig. 11b) and high La/Nb and La/Ta ratios of >1.5 and > 22 respectively (Thompson and Morrison 1988), are consistent with derivation of Kahak Mafic rocks from the lithospheric mantle rather than those of OIB-like asthenospheric mantle (Nb/La >1). The mafic plutonic rocks near Kahak have positive $\varepsilon Nd_{(t)}$ values and relatively high $(^{87}Sr/^{86}Sr)_i$ ratios and are similar to island arc magmas (Fig. 9a) which also coincides with the SCLM domain on the isotopic plot. The Kahak mafic-intermediate rocks plot above the MORB-OIB array in the active continental margin field on the Nb/Yb versus Th/Yb diagram (Fig. 11c) of Pearce (2008). High Ba/La and Ba/Th (Labanieh et al. 2012) ratios but relatively low Th/Yb (0.8–1.1) ratios are also consistent with slab-derived fluid enrichment (Labanieh et al. 2012). The Miocene rocks lie farther from the mantle array towards higher $^{87}Sr/^{86}Sr_i$ and $\varepsilon Nd_{(t)}$. This probably indicates higher fluid input (or more crustal contamination) for the Miocene

intrusions. Higher Sr/La ratios (Fig. 11d) in the Kahak Miocene intrusives are also consistent with higher fluid-induced enrichment (Hawkesworth et al. 1997; Jiang et al. 2009) as compared to the Kahak Eocene intrusives.

On the Pb isotopic plot (Fig. 9b), the Kahak intrusive rocks lie between the fields of MORB, and global subducting sediment (GLOSS) and within the arc volcanic field. It seems that the higher $^{87}Sr/^{86}Sr$ ratios of the Kahak mafic-intermediate intrusive rocks as compared to MORB might be attributed to a flux of slab-derived fluids involving subducted marine sediments from the Neo-Tethyan oceanic slab. Low Ce/Pb and high Th/Nb ratios relative to MORB (Ce/Pb ~ 25, Th/Nb ~ 0·05) are also evidences of sedimentary input into the mantle source (Gertisser and Keller 2003).

The Pb isotopic composition of the Kahak mafic-intermediate rocks lie within that of EMII (Fig. 9b). Enriched mantle component EMII has negative Nb-Ta anomalies and lower $(Ta/La)_N$ ratios than $(Hf/Sm)_N$ (Hart 1984; Palacz and Saunders 1986). EMII is believed to be the result of sediment contamination of the mantle during subduction (e.g., Kimura et al. 2016). The subducted Neotethys oceanic slab has been considered a source of EMII components elsewhere in the UDMA (Honarmand et al. 2014) and probably played a role here as well.

Tectonic setting and implications

The age and geochemistry of gabbroic rocks can be used as tracers of a region's tectonic evolution. The Cenozoic gabbros to diorites in the Kahak area formed in two age ranges from ~53–38 Myr and 23–20 Myr and can be used to constrain the geodynamic evolution of the UDMA. The Eocene and Miocene Kahak mafic-intermediate bodies lack a highly alkaline nature and strong HFSE enrichment; therefore, they are unlikely to have formed in a post-collisional setting (Harris et al. 1986). Instead, they are likely to have been the products of magmatism before collision of the Arabian and central Iran plate. The collision time remains ambiguous, but probably postdates the Early Miocene (Berberian and Berberian 1981; Verdel et al. 2011).

It is believed that the Eocene magmatic rocks in the UDMA formed in a "flare-up" stage that followed flat slab subduction in the Cretaceous (Berberian and King 1981; Alavi 1994; Omrani et al. 2008; Verdel et al. 2011). Verdel et al. (2007, 2011) proposed that regional extension and a magmatic flare-up from ~55 Myr (Latest Paleocene-Early Eocene) until ~37 Myr (Late Eocene) were important events in Iran. Verdel et al. believed that a main phase of magmatism spanned most or all of the Eocene that occurred quite possibly as multiple pulses. They suggested that the Eocene extension and lithospheric thinning might have been accompanied by decompression melting of upwelling hydrous mantle within the subduction zone. Shafaii Moghadam et al. (2015) also proposed that Eocene extension coincided with lithospheric delamination and rapid exhumation of core complexes in central Iran. Pang et al. (2013) and Sepidbar et al. (2018) concluded that Late Paleocene-Eocene flare-up volcanism in east and northeast Iran had chemical characteristics typical of continental arc magmatism. They concluded that later Eocene-Oligocene magmatism in northeast Iran was associated with extension above the subducting Neotethyan ocean slab.

Wide, continuous zircon crystallization age ranges of the Eocene Kahak magmatic rocks (i.e., ~53–38 Myr) are in line with the flare-up hypothesis of Verdel et al. (2011) indicating that the magmas have been furnished over a protracted period of time. Because of the low viscosity of mafic melts, which make them difficult to stagnate, the magmatism probably occurred as multiple continued magmatic events. Three Eocene magmatic events of 1.4 Myr, 5.4 Myr and 6.9 Myr durations are implied by the spectra of zircon ages in three samples from the Kahak area as follow; 46.5–53.4 Myr (VS22), 40.6–46.0 Myr (TS8) and 37.7–39.1 Myr (NA5) (Fig. S3 in the ESM). The compositions and ages of the Eocene Kahak mafic-intermediate intrusions are consistent with the Eocene crustal extension and melting above a subduction zone where the fluids released from a low-dip slab slightly metasomatized the lithospheric mantle. Development of shallow marine Oligocene and Miocene deposits, Lower Red and Qom Formations, across Iran including UDMA (Karevan et al. 2015; Behforouzi and Safari 2011; Vaziri and Sfidari 2012) is consistent with the findings of the present study that infers extensional framework for the Eocene to Miocene magmatism in the Kahak area.

Eocene mafic rocks from the study area are tholeiitic both in major element (Figs. 6c, d) and trace element (Fig. 8c) geochemistry. Tholeiitic magmatism (i.e., of MORB types), though typical of oceanic magmatism, also occurs in the very early stage of suprasubduction zone magmatism (Dilek et al. 2008; Dilek and Furnes 2009). The enriched magmas rose and fractionated olivine and clinopyroxene and were finally solidified as Eocene Naragh and Veshnaveh intrusions (Fig. 12a).

Berberian and King (1981), based on isotopic and elemental geochemistry, considered Oligo-Miocene plutonic rocks from the UDMA as representing Neotethyan subduction-related magmatism. Omrani et al. (2008) and Agard et al. (2011) based on a presumed 'lack or paucity of the Oligocene magmatic rocks' in the UDMA, considered Oligocene as a dormant period. However, recent studies in the UDMA (e.g., Verdel et al. 2011; Chiu et al. 2013; Yeaganehfar et al. 2013; Ghorbani et al. 2014; Honarmand et al. 2014; Babazadeh et al. 2017) have found numerous Oligocene and Miocene volcanic and plutonic bodies with typical subduction-related signatures. These findings point to the fact that Oligocene was not magmatically dormant. Oligocene magmatism has been attributed, almost unanimously, to mantle-plume upwelling that accompanied Neo-

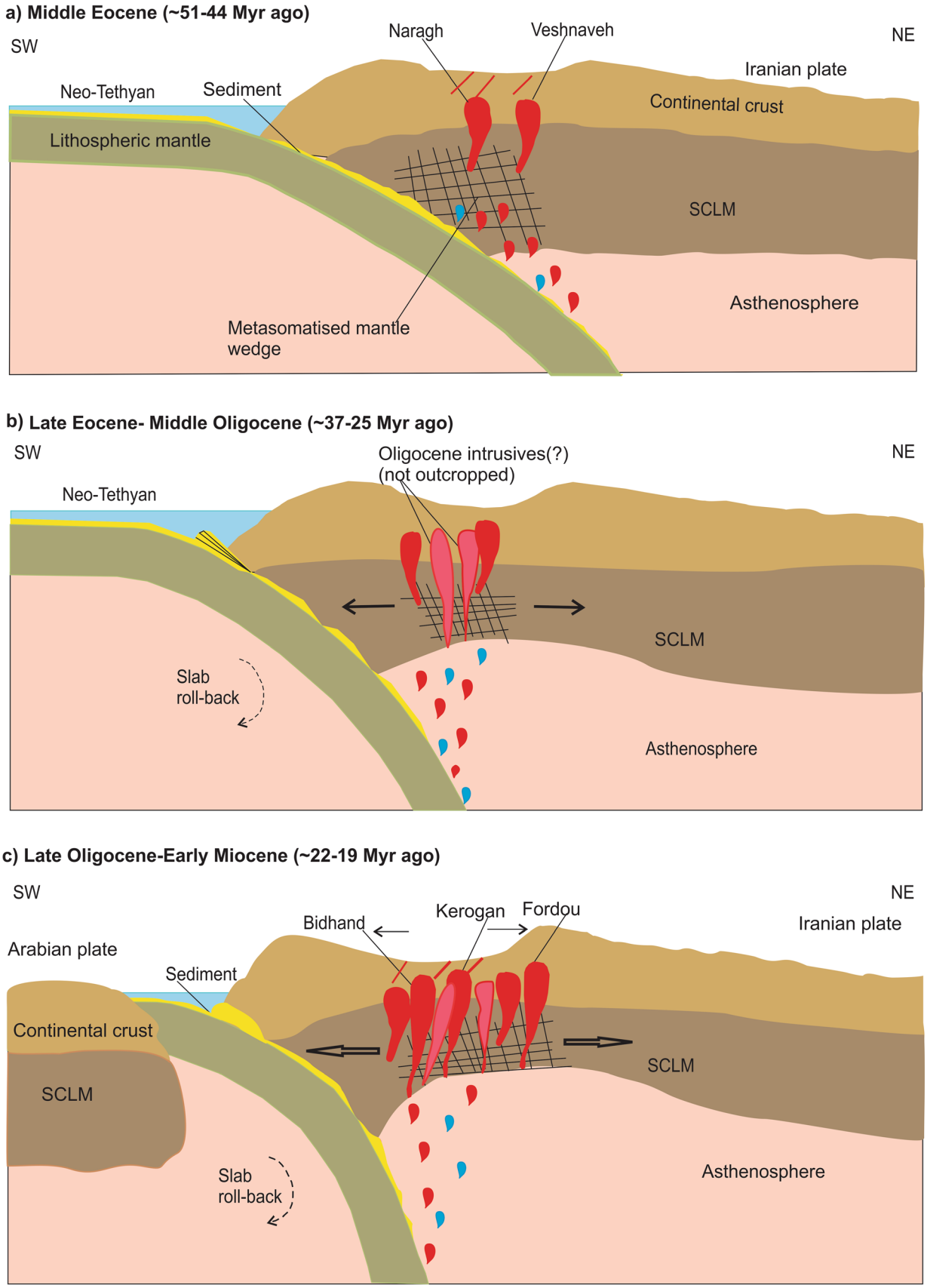

Fig. 12 Schematic cross sections of central Iran delineating major features of the geodynamic settings for petrogenesis of the Eocene, Oligocene, and Miocene Kahak mafic-intermediate intrusive rocks. SCLM = Subcontinental lithospheric mantle

Tethyan slab roll-back. Therefore, it is believed that during the Oligocene to early Miocene (i.e., 38–20 Myr), the Neo-Tethyan oceanic lithosphere was still present, though passively, beneath the central Iranian micro continental plate, which resulted in the magmatic rocks in the UDMA. The presence of 25 Ma to 37 Ma zircons in the younger plutonic rocks (Miocene samples KRA31 and KR32) indicate that zircons were contributed by 25 Ma to 37 Ma country rocks which were assimilated by younger magmas. Therefore, intrusions of 25 Ma to 37 Ma (i.e., mainly of Oligocene age) probably formed in the Kahak area but are not exposed (Fig. 12b).

The lower HREE contents and more spikey LILE patterns of the Miocene Kahak mafic-intermediate rocks as compared to the Eocene intrusions are attributed to an origin deeper in the subcontinental mantle and with a higher flux of subduction zone fluids. We suggest that continued intra-arc extension, possibly prompted by slab roll back, triggered partial malting of a deeper segment of the SCLM. In some nearby areas, slab roll back was steep enough to trigger asthenosphere upwelling according to Ghorbani et al. (2014), who reported high Nb-Ta basalts of Miocene age close to the Kahak intrusions and ascribed the basalts to derivation from an asthenospheric plume developed as a consequence of slab roll back (Fig. 12c). The parental magmas of the Miocene intrusions fractionated dominantly by removal of olivine and clinopyroxene to develop the range of compositions exposed today. Delayed plagioclase fractionation and its later accumulation lead to high Al_2O_3 and CaO in Miocene Kahak intrusions.

Conclusions

A series of Eocene and Miocene gabbros to diorites in the Kahak region provide an excellent opportunity for evaluating the geodynamic evolution of the Cenozoic Urumieh-Dokhtar Magmatic Assemblage (UDMA) of central Iran. The major conclusions derived from the present study of them are: (i) The Veshnaveh and Naragh gabbroic diorites and diorites formed in the Eocene (weighted mean ages of 51.0 ± 4.8 Ma, 45.9 ± 1.8 Ma, and 44.7 ± 1.3 Ma). The wide time span the zircon ages cover (i.e., ~53 Ma −38 Ma), indicate that the Eocene Kahak mafic rocks are produced by a continuous supply of magma batches in a protracted period of time. Three continued magmatic events of 46.5–53.4 Myr, 40.6–46.0 Myr and 37.7–39.1 Myr time spans are indicated by the zircons retrieved from samples VS22, TS8 and NA5 respectively. (ii) The Kerogan, Bidhand, and Fordou gabbros intruded in the Miocene (21.4 ± 0.6 Ma 21.9 ± 0.6 Ma, and 20.5 ± 1 Ma). The presence of 25–37 Ma zircons in the Miocene intrusions imply that Oligocene intrusions are also present in the study area, although they are not exposed. (iii) Sr-Nd isotope ratios lie to the right of the mantle array with positive $\varepsilon Nd_{(t)}$ (+1.4 to +6.2) and are similar to subduction-related island arc rocks with insignificant crustal contamination. Pb isotopic ratios for the Kahak mafic- intermediate intrusions lie near the EMII field, believed to be the result of sediment (i.e., Neotethyan slab sediments) contamination of the mantle. (iv) The Miocene Kahak intrusions have lower Nb-Ta and HREE abundances and higher lithophile element concentrations than their Eocene counterparts. Compared to the Eocene, Miocene partial melting may have occurred in the deeper levels of the subcontinental lithospheric mantle, where slab-derived fluids were more effective, producing more mafic magmas with stronger enrichments of fluid-soluble elements like Cs, Rb, and Ba.

Supplementary Information The online version contains supplementary material available at https://doi.org/10.1007/s00710-021-00745-z.

Acknowledgements The present work is part of the Ph.D. thesis of S.M. who acknowledges the support she received from the staff and students of Tarbiat Modares University, Brigham University, and the China University of Geoscience (CUG) where she spent her 6-month sabbatical. Colby Pearson and Shane Dailey from Brigham Young University are acknowledged for their help with the XRF analyses. Duan Dengfie from China University of Geosciences is acknowledged for the ICP-MS, Sr-Nd and Pb isotope, EMPA, and zircon U-Pb dating analyses. Constructive comments of two anonymous reviewers and editor Qiang Wang are gratefully acknowledged.

References

Aftabi A, Atapour H (2000) Regional aspects of shoshonitic volcanism in Iran. Episodes 23:119–125

Agard P, Omrani J, Jolivet J, Whitechurch H, Vrielynck B, Spakman W, Monié P, Meyer B, Wortel R (2011) Zagros orogeny: a subduction-dominated process. Geol Mag 148:692–725

Alavi M (1994) Tectonics of the Zagros orogenic belt of Iran: new data and interpretations. Tectonophysics. 229:211–238

Alavi M (1996) Tectonostratigraphic synthesis and structural style of the Alborz Mountain system in northern Iran. J Geodyn 21:1–33

Aldanmaz E, Pearce JA, Thirlwall MF, Mitchell JG (2000) Petrogenetic evolution of late Cenozoic, post-collision volcanism in western Anatolia. Turkey. J Volcanol Geotherm Res 102(1–2):67–95

Allen M, Jackson J, Walker R (2004) Late Cenozoic reorganization of the Arabia-Eurasia collision and the comparison of short-term and long-term deformation rates. Tectonics 23:1–16

Aoki K, Shiba I (1993) Pyroxene from lherzolite inclusions of Itinom egata Japan. Lithos 6:41–51

Arvin M, Pan Y, Dargahi S, Malekizadeh A, Babaei A (2007) Petrochemistry of the Siah-Kuh granitoid stock southwest of Kerman, Iran: implications for initiation of Neotethys Subduction. J Asian Earth Sci 30:474–489

Babazadeh S, Ghorbani MR, Bröcker M, D'Antonio M, Cottle J, Gebbing T, Carmine Mazzeo F, Ahmadi P (2017) Late Oligocene-Miocene mantleupwelling and interaction inferred from mantle signatures in gabbroic to granitic rocks from the Urumieh-Dokhtar arc, south Ardestan, Iran. Int Geol Rev 59(12):1590–1608

Babazadeh S, Ghorbani MR, Cottle JM, Bröcker M (2018) Multistage tectono-magmatic evolution of the central Urumieh-Dokhtar

magmatic arc, south Ardestan, Iran: Insights from zircon geochronology and geochemistry. Geol J 54:2447–2471
Ballato P, Uba CE, Landgraf A, Strecker MR, Sudo M, Stockli DF, Friedrich A, Tabatabaei SH (2011) Arabia-Eurasia continental collision: insights from late tertiary foreland basin evolution in the Alborz Mountains, northern Iran. Geol Soc Am Bull 123:106–131
Bau M (1996) Controls on the fractionation of isovalent trace elements in magmatic and aqueous systems: evidence from Y/ho, Zr/Hf, and lanthanide tetrad effect. Contrib Mineral Petrol 123:323–333
Bau M, Dulski P, Moller P (1995) Yttrium and holmium in South Pacific seawater: vertical distribution and possible fractionation mechanisms. Chem Erde 55:1–15
Behforouzi E, Safari A (2011) Biostratigraphy and paleoecology of the Qom formation in Chenar area (northwestern Kashan), Iran. Rev Mex de Cienc Geol 28(3):555–565
Belousova E, Griffin WL, O'Reilly SY, Fisher NL (2002) Igneous zircon: trace element composition as an indicator of source rock type. Contrib Mineral Petrol 143(5):602–622
Ben Othman D, White WM, Patchett J (1989) The geochemistry of marine sediments, island arc magma genesis and crust-mantle recycling. Earth Planet Sci Lett 94:1–24
Berberian F, Berberian M (1981) Tectono-plutonic episodes in Iran. Geological Survey of Iran, Report 52:566–593
Berberian M, King GCP (1981) Towards a paleogeography and tectonic evolution of Iran. Can J Earth Sci 18:210–265
Berberian F, Muir ID, Pankhurst RJ, Berberian M (1982) Late Cretaceous and early Miocene Andean-type plutonic activity in northern Makran and central Iran. J Geol Soc London 139:605–614
Boynton WV (1984) Geochemistry of Rare Earth Elements: Meteorite Studies. In: Henderson P (ed) Rare Earth Element Geochemistry. Elsevier, New York, pp 63–114. https://doi.org/10.1016/B978-0-444-42148-7.50008-3
Cann JR (1970) Rb, Sr, Y, Zr, Nb in some ocean floor basaltic rocks. Earth Planet Sci Lett 10:7–11
Castillo PR, Janney PE, Solidum RU (1999) Petrology and geochemistry of Camiguin island, southern Philippines: insights to the source of adakites and other lavas in a complex arc setting. Contrib Mineral Petrol 134:33–51
Chen W, Arculus RJ (1995) Geochemical and isotopic characteristics of lower crustal xenoliths, San Francisco Volcanic Field, Arizona, U.S.A. Lithos 36:203–225
Chiu HY, Chung SL, Zarrinkoub MH, Mohammadi SS, Khatib MM, Iizuka Y (2013) Zircon U-Pb age constraints from Iran on the magmatic evolution related to Neotethyan subduction and Zagros orogeny. Lithos 162–163:70–87
De la Roche H, Leterrier J, Grande Claude P, Marchal M (1980) A classification of volcanic and plutonic rocks using R1-R2 diagrams and major element analyses, its relationships and current nomenclature. Chem Geol 29:183–210
Deer WA, Howie RA, Zussman J (1991) An introduction to Rock-forming minerals, 2nd edn. Pearson, Prentice Hall, New York
Defant MJ, Jackson TE, Drummond MS, de Boer JZ, Bellon H, Feigenson MD, Maury RC, Stewart RH (1992) The geochemistry of young volcanism throughout western Panama and southeastern Costa Rica: an overview. J Geol Soc London 149:569–579
Dewey JF, Pitman WC, Ryan WBF, Bonnin J (1973) Plate tectonics and the evolution of the Alpine system. Geol Soc Am Bull 84:3137–3180
Dilek Y, Furnes H (2009) Structure and geochemistry of Tethyan ophiolites and their petrogenesis in subduction rollback systems. Lithos 113:1–20
Dilek Y, Furnes H, Shallo M (2008) Geochemistry of the Jurassic Mirdita Ophiolite (Albania) and the MORB to SSZ evolution of a marginal basin oceanic crust. Lithos 100:174–209
Dupré B, Allègre CJ (1983) Pb-Sr isotope variation in Indian Ocean basalts and mixing phenomena. Nature 303:142–146
Ernst WG, Liu J (1998) Experimental phase-equilibrium study of Al- and Ti-contents of calcic amphibole in MORB-A. Semiquantitative thermobarometer. Am Mineral 83:952–969
Eyuboglu Y (2015) Petrogenesis and U–Pb zircon chronology of felsic tuffs interbedded with turbidites (Eastern Pontides Orogenic Belt, NE Turkey): Implications for Mesozoic geodynamic evolution of the eastern Mediterranean region and accumulation rates of turbidite sequences. Lithos 212–215:74–92
Fitton JG, James D, Leeman WP (1991) Basic magmatism associated with late Cenozoic extension in the Western United States: compositional variations in space and time. J Geophys Res Solid Earth 96:13693–13712
Garfunkel Z (2008) Formation of continental flood volcanism the perspective of setting of melting. Lithos 100:49–65
George R, Rogers N (2002) Plume dynamics beneath the African plate inferred from the geochemistry of the tertiary basalts of southern Ethiopia. Contrib Mineral Petrol 144:286–304
Gertisser R, Keller J (2003) Trace element and Sr, Nd, Pb and O isotope variations in medium-K and high-K volcanic rocks from Merapi volcano, Central Java, Indonesia: evidence for the involvement of subducted sediments in Sunda arc magma genesis. J Petrol 4:457–489
Ghalamghash G, Babakhani A (1996) Geological map of Kahak: sheet 6158, Ministry of Mines and Metals. Geological Survy of Iran, Tehran
Ghasemi A, Talbot CJ (2006) A new tectonic scenario for the Sanandaj - Sirjan zone (Iran). J Asian Earth Sci 26:683–693
Ghorbani MR (2006) Lead enrichment in Neotethyan volcanic rocks from Iran: the implications of a descending slab. Geochem J 40:557–568
Ghorbani MR, Bezenjani RN (2011) Slab partial melts from the metasomatizing agent to adakite, Tafresh Eocene volcanic rocks, Iran. Island Arc 20:188–202
Ghorbani MR, Graham IT, Ghaderi M (2014) Oligocene-Miocene geodynamic evolution of the central part of Urumieh-Dokhtar arc of Iran. Int Geol Rev 56:1039–1050
Gill R (2010) Igneous rocks and processes: a practical guide. John Wiley & Sons Ltd Publication, Uk, p 428
Hajian J (2001) Geology of Tafresh: geological and mineralogical exploration survey of Iran, Tehran, Report No 82
Hamelin B, Dupré B, Allègre CJ (1985) Pb-Sr-Nd isotopic data of Indian Ocean ridges: new evidence of large-scale mapping of mantle heterogeneities. Earth Planet Sci Lett 76:288–298
Hanchar JM, Van Wastrenen W (2007) Rare earth element behavior in zircon-melt system. Elements 3:37–42
Harris NBW, Pearce JA, Tindle AG (1986) Geochemical characteristics of collision-zone magmatism. In: M. P. Coward and A. C. Ries, (Eds): Collision Tectonics Geol Soc Spec Publ 19:67–81
Hart SR (1984) The Dupal anomaly: a large-scale isotopic anomaly, in the southern hemisphere. Nature 309:753–756
Hart SR, Gerlach DC, White WM (1986) A possible new Sr-Nd-Pb mantle array and consequences for mantle mixing. Geochim Cosmochim Acta 50(7):1551–1557
Hassanzadeh J (1993) Metallogenic and tectono-magmatic events in the SE sector of the Cenozoic active continental margin of Iran (Shahr-e Babak area, Kerman province). Unpublished Ph.D. thesis, University of California, Los Angeles, p 204
Hassanzadeh J, Stockli DF, Horton BK, Axen GJ, Stockli LD, Grove M, Schmitt AK, Walker JD (2008) U-Pb zircon geochronology of late Neoproterozoic-early Cambrian granitoids in Iran: implications for paleogeography, magmatism, and exhumation history of Iranian basement. Tectonophysics 451:71–96
Hawkesworth CJ, Turner SP, McDermott F, Peate DW, van Calsteren P (1997) U-Th isotopes in arc magmas: implications for element transfer from the subducted crust. Science 276:551–555

Honarmand M, Rashidnejad Omran N, Neubauer F, Emami MH, Nabatian G, Liue X, Dong Y, von Quadt A, Chen B (2014) Laser-ICP-MS U-Pb zircon ages and geochemical and Sr-Nd-Pb isotopic compositions of the Niyasar plutonic complex, Iran: constraints on petrogenesis and tectonic evolution. Int Geol Rev 56:104–132

Hoskin PWO, Schaltegger U (2003) The composition of zircon and igneous and metamorphic petrogenesis. Rev Mineral Geochem 53: 27–62

Irvine TN, Baragar WRA (1971) A Guide to the Chemical Classification of the Common Volcanic Rocks. Can J Earth Sci 8:523–548

Jiang YH, Jiang SY, Dai BZ, Liao SY, Zhao KD, Ling HF (2009) Middle to late Jurassic felsic and mafic-intermediate magmatism in southern Hunan province, Southeast China: implications for a continental arc to rifting. Lithos 107:185–204

Kamei A, Owada M, Nagao T, Shiraki K (2004) High-mg diorites derived from sanukitic HMA magmas, Kyushu Island, Southwest Japan arc: evidence from clinopyroxene and whole rock compositions. Lithos 75:359–371

Kananian A, Sarjoughian F, Nadimi A, Ahmadian J, Ling W (2014) Geochemical characteristics of the Kuh-e Dom intrusion, Urumieh-Dokhtar magmatic arc (Iran): implications for source regions and magmatic evolution. J Asian Earth Sci 90:137–148

Karevan M, Vaziri-Moghaddam H, Mahboubi A, Moussavi-Harami R (2015) Biostratigraphy and paleo-ecological reconstruction on Scleractinian reef corals of Rupelian-Chattian succession (Qom formation) in northeast of Delijan area. Geopersia 4(1):11–24

Karsli O, Dokuz A, Uysal I, Aydin F, Chen B, Kandemir R, Wijbrans J (2010) Relative contributions of crust and mantle to generation of Campanian high-K calc-alkaline I type granitoids in a subduction setting, with special reference to the Harsit pluton, eastern Turkey. Contrib Mineral Petrol 160:467–487

Kimura JL, Gill JB, Sokra S, Van Kehen PE, Kawabata H (2016) Origin of geochemical mantle components: Role of subduction filter. Geochem Geophys Geosys 17:3289–3325

Labanieh S, Chauvel C, Germa A, Quidelleur X (2012) Martinique: a clear case for sediment melting and slab dehydration as a function of distance to the trench. J Petrol 53:2441–2464

Leake BE, Woolley AR, Arps CES, Birch WD, Gilbert MC, Grice JD, Hawthorne FC, Kato A, Kisch HJ, Krivovichev VG, Linthout K, Laird J, Mandarino J, Maresch WV, Nickel EH, Rock NMS, Schumacher JC, Smith DC, Tephenson NCN, Ungaretti L, Whittaker EJW, Youzhi G (1997) Nomenclature of amphiboles: report of the subcommittee on amphiboles of the international mineralogical association, commission on new minerals and mineral names. Can Mineral 35:219–246

Liu YS, Gao S, Hu ZC, Gao CG, Zong KQ, Wang DB (2010a) Continental and oceanic crust recycling-induced melt-peridotite interactions in the trans-North China Orogen: U-Pb dating, Hf isotopes and trace elements in zircons of mantle xenoliths. J Petrol 51(1 and 2):537–571

Liu YS, Hu ZC, Gao S, Gunter D, Xu J, Gao CG, Chen HH (2008) In situ analysis of major and trace elements of anhydrous minerals by LA-ICP-MS without applying an internal standard. Chem Geol 257:34–43

Liu YS, Hu ZC, Zong KQ, Gao CG, Gao S, Xu J, Chen HH (2010b) Reappraisement and refinement of zircon U-Pb isotope and trace element analyses by LA-ICP-MS. Chin Sci Bull 55(15):1535–1546

Ludwig KR (2003) ISOPLOT 3.00: a Geochronological toolkit for Microsoft excel. Berkeley Geochronology Center, Berkeley

Middlemost EAK (1994) Naming materials in the magma igneous rock system. Earth-Sci Rev 37:215–224

Miyashiro A (1974) Volcanic rocks series in island arcs and active continental margins. Am J Sci 274:321–355

Mohajjel M, Fergusson CL (2014) Jurassic to Cenozoic tectonics of the Zagros Orogen in northwestern Iran. Int Geol Rev 56:263–287

Moradian Shahr-e-babaky A (1997) Geochemistry, Geochronology and Petrography of Feldspathoid Bearing Rocks in Urumieh-Dokhtar Volcanic Belt, Iran, Unpublished PhD thesis, University of Wollongong, Australia, p 412

Morimoto N (1988) Nomenclature of pyroxenes. Fortschr Mineral 66: 237–252

Mouthereau F, Lacombe O, Vergés J (2012) Building the Zagros collisional orogen: timing, strain distribution and the dynamics of Arabia /Eurasia plate convergence. Tectonophysics 532–535:27–60

Nouri F, Azizi H, Stern RJ, Asahara Y, Khodaparast S, Madanipour S, Amamoto Y (2018) Zircon U-Pb dating, geochemistry and evolution of the late Eocene Saveh magmatic complex, Central Iran: partial melts of sub-continental lithospheric mantle and magmatic differentiation. Lithos 314–315:274–292

Omrani J, Agard P, Whitechurch H, Benoit M, Prouteau G, Jolivet L (2008) Arc-magmatism and subduction history beneath the Zagros Mountains, Iran: a new report of adakites. Lithos 106:380–398

Palacz ZA, Saunders AD (1986) Coupled trace element and isotope enrichment in the Cook–Austral– Samoa islands, southwest Pacific. Earth Planet Sci Lett 79:270–280

Pang KN, Chung SL, Zarrinkoub MH, Khatib MM, Mohammadi SS, Chiu HY, Chu CH, Lee HY, Lo CH (2013) Eocene-Oligocene post-collisional magmatism in the Lut-Sistan region, eastern Iran: magma genesis and tectonic implications. Lithos 180:234–251

Pearce JA (2008) Geochemical fingerprinting of oceanic basalts with applications to ophiolite classification and the search for Archean oceanic crust. Lithos 100:14–48

Plank T (2005) Constraints from thorium/lanthanum on sediment recycling at subduction zones and the evolution of the continents. J Petrol 46:921–944

Polat A, Hofmann AW (2003) Alteration and geochemical patterns in the 3.7–3.8 Ga Isua greenstone belt. West Greenland. Precambrian Res 126:197–218

Pu W, Gao J, Zhao K, Ling H, Jiang S (2005) Separation method of Rb-Sr, Sm-Nd using DCTA and HIBA. J Nanjing Univ (Natural Sciences) 41:445–450

Pu W, Zhao K, Ling H, Jiang S (2004) High precision Nd isotope measurement by triton TI mass spectrometry. Acta Geol Sin 25:271–274

Rehkamper M, Hofmann AW (1997) Recycled ocean crust and sediment in Indian Ocean MORB. Earth Planet Sci Lett 147(1–4):93–106

Ramezani J, Tucker RD (2003) The Saghand region, Central Iran: U-Pb geochronology, petrogenesis and implications for Gondwana tectonics. Am J Sci 303:622–665

Rezaei-Kahkhaei M, Galindo C, Pankhurst RJ, Esmaeily D (2011) Magmatic differentiation in the calc-alkaline Khalkhab-Neshveh pluton, Central Iran. J Asian Earth Sci 42:499–514

Rezeau H, Moritz R, Leuthold J, Hovakimyan S, Tayan R, Chiaradia M (2017) 30 Myr of Cenozoic magmatism along the Tethyan margin during Arabia-Eurasia accretionary orogenesis (Meghri-Ordubad pluton, southernmost lesser Caucasus). Lithos 288:108–124

Rollinson HR (1993) Using geochemical data: evaluation, presentation, interpretation. Longman, New York

Rudnick RL, Gao S (2003) Composition of the continental crust. Treatise Geochemistry 3:1–64

Saunders AD (2005) Large igneous provinces: origin and environmental consequences. Elements 1:259–263

Sepidbar F, Mirnejad H, Ma C, Shafaii Moghadam H (2018) Identification of Eocene-Oligocene magmatic pulses associated with flare-up in East Iran: timing and sources. Gondwana Res 57:141–156

Shafaii Moghadam H, Li XH, Ling XX, Santos JF, Rj S, Li QL, Ghorbani G (2015) Eocene Kashmar granitoids (NE Iran): Petrogenetic constraints from U-Pb zircon geochronology and isotope geochemistry. Lithos 216-217:118–135

Smith EI, Sánchez A, Walker JD, Wang K (1999) Geochemistry of mafic magmas in the Hurricane volcanic field, Utah: implications for small

and large-scale chemical variability of the lithospheric mantle. Geol J 107:433–448

Soesoo A (1997) A multivariate statistical analysis of clinopyroxene composition: empirical coordinates for the crystallisation PT-estimations. Geol Soc Sweden 119:55–60

Springer W, Seck HA (1997) Partial fusion of basic granulites at 5 to 15 kbar: implications for the origin of TTG magmas. Contrib Mineral Petrol 127:30–45

Sun SS, McDonough WF (1989) Chemical and isotopic systematics of oceanic basalts: implications for mantle composition and processes. In: Saunders AD, Norry MJ (eds) Magmatism in ocean basins, vol 42. Geological Society of London, Special Publication, pp 313–345

Takamasa A, Ichinakai S (2009) Contamination introduced during rock sample powdering: effects from different mill materials on trace element contamination. J Geochem 43:389–394

Tanaka T, Togashi S, Kamioka H, Amakawa H, Kagami H, Hamamoto T, Yuhara M, Orihashi Y, Yoneda S, Shimizu H, Kunimaru T, Takahashi K, Yanagi T, Nakano T, Fujimaki H, Shinjo R, Asahara Y, Tanimizu M, Dragusanu C (2000) JNdi-1: a neodymium isotopic reference in consistency with LaJolla neodymium. Chem Geol 168(3–4):279–281

Tang X, Zhang JC, Shan YS, Xiong JY (2012) Upper Paleozoic coal measures and nconventional natural gas systems of the Ordos Basin. China. Geosci Front 3(6):863–873

Taylor SR, McLennan SM (1995) The geochemical evolution of the continental crust. Rev Geophys 33:241–265

Thompson RN, Morrison MA (1988) Asthenospheric and lower lithospheric mantle contributions to continental extension magmatism: an example from the British Tertiary Province. Chem Geol 68:1–15

Todt W, Cliff RA, Hanser A, Hofmann AW (1996) Evaluation of ^{202}Pb-^{205}Pb double spike for high-precision lead isotope analysis. Earth processes: Reading the isotopic code. Geophys Monograph Union 95:429–437

Turner S, Foden J (2001) U, Th and Ra disequilibria, Sr, Nd and Pb isotope and trace element variations in Sunda arc lavas: predominance of a subducted sediment component. Contrib Mineral Petrol 142:43–57

Vaziri MR, Sfidari E (2012) The Tethyan seaway Iranian plate Oligo-Miocene deposits (the Qom formation): distribution of Rupelian (early Oligocene) and evaporate deposits as evidences for timing and trending of opening andclosure of the Tethyan seaway. Carbonate Evaporite 28:321–345

Verdel C, Wernicke BP, Hassanzadeh J, Guest B (2011) A Paleogene extensional arc flare -up in Iran. Tectonics 30:1–20

Verdel C, Wernicke BP, Ramezani J, Hassanzadeh J, Renne PR, Spell TL (2007) Geology and thermochronology of tertiary cordilleran-style metamorphic core complexes in the Saghand region of Central Iran. Geol Soc Am Bull 119:961–977

Wang BD, Wang LQ, Chung SL, Chen JL, Yin FG, Liu H, Li XB, Chen LK (2016) Evolution of the Bangong-Nujiang Tethyan Ocean: insights from the geochronology and geochemistry of mafic-intermediate rocks within ophiolites. Lithos 245:18–33

White WM, Hofmann AW (1982) Sr and Nd isotope geochemistry of oceanic basalts and mantle evolution. Nature 296:821–825

Whitford DJ, White WM, Jezek PA (1981) Neodymium isotopic composition of Quaternary island arc lavas from Indonesia. Geochim Cosmochim Acta 45:989–995

Whitney DL, Evan BW (2010) Abbreviations for names of rock-forming minerals. Am Mineral 95:185–187

Woodhead JD, Eggins SM, Johnson RW (1998) Magma genesis in the New Britain Island arc: further insights into melting and mass transfer processes. J Petrol 39:1641–1668

Wu YB, Zheng YF (2004) Genesis of zircon and its constraints on interpretation of U-Pb age. Chin Sci Bull 49(15):1554–1569

Yamasaki T (2018) Contamination from mortars and mills during laboratory crushing and pulverizing. Bull Geol Surv Japan 69(3):201–210

Yeganehfar H, Ghorbani M, Shinjo R, Ghaderi M (2013) Magmatic and geodynamic evolution of Urumieh-Dokhtar basic volcanism, Central Iran: major, trace element, isotopic, and geochronologic implications. Int Geol Rev 55:767–786

Zhang FL, Zhu M, Wang CY (2007) Parameters optimization in the planetary ball milling of nanostructured tungsten carbide/cobalt powder. Int J Refract Met Hard Mater 26:329–333

Zhang J, Amakawa H, Nozaki Y (1994) The comparative behaviors of yttrium and lanthanides in the seawater of the North Pacific. Geophys Res Lett 21:2677–2680

Zhang RX, Yang SY (2016) A mathematical model for determining carbon coating thickness and its application in electron probe micro-analysis. Microsc Microanal 22:1374–1380